Scientia Iranica A (2019) 26(4), 2079–2099

Sharif University of Technology
Scientia Iranica
Transactions A: Civil Engineering
http://scientiairanica.sharif.edu

Invited Paper

Finite element model and size-dependent stability analysis of boron nitride and silicon carbide nanowires/nanotubes

H.M. Numanoğlu, K. Mercan, and Ö. Civalek*

Division of Mechanics, Department of Civil Engineering, Faculty of Engineering, Akdeniz University, 07058 Antalya, Turkey.

Received 21 December 2018; received in revised form 20 February 2019; accepted 6 April 2019

KEYWORDS
Boron nitride;
Silicon carbide;
Nanotube;
Nanowire;
Buckling.

Abstract. In the present paper, stability analysis of boron nitride and silicon carbide nanotubes/nanowires is carried out using different size-effective theories, finite element method, and computer software. Size-effective theories used in this paper include Modified Couple Stress Theory (MCST), Modified Strain Gradient Theory (MSGT), Nonlocal Elasticity Theory (NET), Surface Elasticity Theory (SET), and Nonlocal Surface Elasticity Theory (NSET). As for the computer software, ANSYS and COMSOL multiphysics are used. Comparative results of theories and software and literature are given in the result section. Comparative results are in good harmony. In conclusion, it is clearly seen that the nonlocal elasticity theory yields the lowest results for every modes and structures, while the modified strain gradient theory yields the highest results.

1. Introduction

Nanotubes and nanowires are used in a wide range of scientific areas since their discovery. The usage areas of nanotubes and nanowires can be divided into two main groups: 'current' and 'potential' usage areas. With its ultimate mechanical and adjustable geometric parameters, the second group of 'potential usage area' can be described almost as 'limitless'. On the other hand, the current usage areas of nanotubes and nanowires are in bulk state, which means a mass of unorganized nanostructures [1-3]. Nanostructures in the bulk form are widely used as composite fibers to improve the mechanical, electrical, and thermal properties of polymers [4]. For example, one of the largest companies in the sport equipment-producing field that invests in futuristic research and developments seriously has produced carbon nanotube (CNT) reinforced bicycle components. By reinforcing bicycle components, they developed very high strain-stress resistance in addition to massive loss in weight [5]. Another current application of nanostructures is to absorb gases by their active surface area [6]. Absorbing gases has vital importance for environmental monitoring and the future of this planet. Otherwise, with ongoing improvements in nano-scale technology, nanostructures promise limitless, highly beneficial usage areas. In addition, new nanostructures such as three-dimensional nanoblocks are studied. These 3D nanoblocks are composed of nanostructures and have a limited size up to 1 mm in all dimensions. A new method was researched and published by Lalwani et al., which uses single- and multi-walled carbon nanotubes to eventually produce nanoblocks [7]. These developments can be described as promising for new supercapasitors, batteries with

*. *Corresponding author. Tel.: +902423106319*
E-mail addresses: metin_numanoglu@hotmail.com (H.M. Numanoğlu); mercankadir@akdeniz.edu.tr (K. Mercan); civalek@yahoo.com (Ö. Civalek)

doi: 10.24200/sci.2019.52517.2754

super energy storage capacity, transistors used for field emission, and catalysts with high performance [8].

In related literature, the history of nanotubes is widely based on the research published by Iijima about nanotubes in 1991 [9]. However, this literature comprises older studies on nanotubes. These studies have also determined nanotubes without identifying their relevant structures. In this regard, the first research conducted was published by Watson and Kaufmann in 1946 [10]. Watson and Kaufmann investigated synthesis of carbon nanotube structures under the rubric of 'tubular carbon'. The 'tubular carbon' was obtained with a diameter of almost 100 nm by examining cuprene over fine copper oxide catalyst up to 300°C. Following six years of research published by Watson and Kaufmann, Radushkevich and Lukyanovich published primary images of carbon nanotubes with diameters ranging from 30 nm to 50 nm by transmission electron microscopy in 1952 [11]. Moreover, the properties, structure, and growth methods of nanostructures using arc discharge were analyzed by Bacon in 1960 [12]. Another research was published by Oberlin et al. in 1976 [13]. Oberlin et al. observed carbon fibres by pyrolyzing a mixture of hydrogen and benzene at about 1100°C. The specimens obtained by this chemical vapor-growth method include carbon nanotubes with a diameter of 2-50 nm. These nanotubes are called 'hollow tubes'. Hollow tubes obtained were actually multi-walled carbon nanotubes (MWCNTs). After that, in 1999, John Abrahamson [14] presented a research piece at the 14th Biennial Conference of Carbon at Pennsylvania State University. The research described the carbon nanotubes obtained from arc discharge on carbon anodes. Later, in 1982, the first chirality model of carbon nanotubes was proposed in two combinations [15]. Kolesnik et al. proposed that 'carbon multi-layer tubular crystals', also called multi-walled carbon nanotubes, could be obtained by simply rolling graphene layers into a cylinder. The circular rolling arrangement produces two different structures. These two structures include armchair and chiral nanostructures. On the other hand, the first samples of nanotubes in history were discovered in Damascus steel around 400 years ago. These samples are identified as the first carbon nanotube samples found in history [16].

Recently, with a rise in the popularity of renewable energy for transportation and electronics, studies about carbon nanotube usage for improving the durability, lifespan, and capacity of batteries have started to receive considerable attention [17-28]. Further, in the last decade, studies about the usage of CNT in one of the most effective usage areas, gas sensors, have soared [29-45]. The discovery of CNTs may be a revolutionary point for many application areas such as processor technology, biotechnology, gas/chemical sensors, aerospace technology, etc. [46-48]. Carbon nanotubes have attracted extreme attention due to their mechanical properties that are superior to traditional materials. However, within the foundation of CNTs, scientists have commenced producing nanosized materials with properties superior to CNTs. Later, novel nanotubes/nanowires have been produced based on a different atomic structure, compared to CNTs. Some of these novel nanostructures include boron nitride nanotube (BNNT) and silicon carbide nanotube (SiCNT). To illustrate, in the case of mechanical properties, CNT has Young's modulus around 1 TPa, while BNNT has 1.8 TPa and 0.62 TPa for SiCNT. The Poisson's ratio used for analysis in the current research is 0.37 for SiCNT and 0.25 for BNNT [49-51]. Moreover, CNTs can resist thermal environment up to 600°C, while SiCNT can resist up to 1000°C in the air without any damage [52,53]. BNNT and SiCNT have not been investigated as CNTs had been in the last decade. BNNT has very high potential to deliver drug into blood flow by binding drugs with BNNT [54]. Drugs can then be delivered into the cells for curing cancer cells by killing such cells without damaging healthy ones. Since BNNTs are biocompatible and non-toxic, they can be used as nano-sized drug-delivery cargo vehicles of these anticancer drugs so that they can be delivered directly to cancer cells [55]. Recently, Ferreira et al. investigated the performance of BNNT in the biomedical application area to deliver protein drugs and kill cancer cells by magnetohyperthermia therapy in 2018 [56]. Based on the results obtained by Ferreira et al., BNNT nano-sized structures carried magnetite nanoparticles, and magnetic measurements illustrated that well coercivity and magnetization were observed following the incorporation of magnetite nanoparticles into the BNNT. In addition, the boron nitride structure was investigated in other forms than nanotube. Structures of nanoribbons and nanowires were investigated for use in gas sensors [57]. Although these nanostructures appear analogous, obtaining nanowires is much more laborious than obtaining nanotubes from a technical point of view. Nanotubes are both used in single- and multi-walled forms according to their application area and characteristics [58]. Furthermore, due to their limited resistance to thermal environment, nano-sized technology demands novel nanostructures with superior thermal resistance. Carbon nanotubes and carbon nanowires are nanostructures based on graphene. The thermal resistance of graphene is up to 600°C in air. To address this issue, a new base nanostructure has been obtained and developed. In addition, by overcoming the thermal resistance, the limited usage area of graphene-based nanostructures has expanded. The novel nanostructure is based on Si atoms and named as 'silicene'. Silicene has superior thermal resistance, which can stay stable until

1200°C [59]. Silicene is a layer of hexagonally arranged silicon atoms [60]. Despite superior thermal resistance, silicene has lower Young's modulus, concluding that silicene is mechanically weaker than graphene. To illustrate, the length of Si-Si bond in silicene is 2.29 Å, while the length of the C-C bond is 1.42 Å in graphene and 1.46 Å for boron nitride sheet (base material of BNNT); therefore, silicene can perform higher chemical reactivity than graphene [61]. Longer bond length ends up with lower mechanical properties, making silicene weaker than boron nitride sheet and graphene. Later, silicene and graphene have been composed to obtain a nanostructured material with superior mechanical properties. The novel composition of silicon and carbon atoms formed 'silicon carbide sheet'. NASA Glenn Research Center has cooperated with Rensselaer Polytechnic Institute to produce silicon carbide sheets from carbon and silicon atoms. This cooperation has led to the development of many methods for obtaining silicon carbide sheet, which is itself produced because of the same cooperation. Thermal resistance of silicon carbide sheet made the nanostructure capable to stay stable up to 1000°C with mechanical properties superior to silicene [59]. Silicon carbide nanowires and nanotubes are widely used in gas sensors [62]. These sensors have been used to detect CO and HCN gases in the environment. CO and HCN gases can be absorbed on SiCNWs at Si lattice sites. With the absorption, significant waves in binding energy to charge transfer can easily be observed. The wave in electrical conductivity of SiCNWs results from the chemisorption of gas molecules on the surface of nanowire metal oxides. The main structures of electro-transducers include Field Effect Transistors (FET), resistive gas micro-sensors, and resistive gas sensors [63].

2. Continuum models of nanostructures

Due to the astronomically high cost of micro- and nano-sized experiments, mathematical and continuum models of these structures have always been cost-effective choices for researchers and developers [64-66]. In the literature, many mathematical and continuum mechanic models have been used to model nano- and micro-sized structures. Nanowires have been mostly modeled for conducting analysis using classic and size-effective Euler-Bernoulli and Timoshenko beam theories [67-71]. In addition, shell and plate theories have been used widely to make analysis possible without using any high-tech laboratory or real nanotubes [72-74]. Furthermore, these theories have been used for modeling nano- and micro-composite structures without the need for any lab or real composite materials [75-79]. In addition, various theories have been developed that demonstrate the importance of small-scale effects such as strain gradient theory [80,81], couple stress elasticity theory [81-84], modified couple stress theory [85-88], nonlocal elasticity theory [89,90], and surface elasticity theory [91-95].

In the last decade, many scientists have published a number of research pieces on the subject of the stability and analysis of micro-nanowires and micro-nanotubes. Ansari et al. [96] investigated the buckling behavior of single-walled silicon carbide nanotubes using ANSYS commercial FE code in 2012. After that, in 2013, Arani and Hashemian [97] investigated the surface stress effects on the dynamic stability of double-walled boron nitride nanotubes that convey viscous fluid based on nonlocal shell theory. Later, in 2014, Saljooghi et al. investigated the vibration and buckling behavior of functionally graded beams [98]. They used the reproducing kernel particle method with very good accuracy. In 2015, Darvizeh et al. demonstrated the pre- and post-buckling analyses of beams with Functionally Graded Material (FGM), a mixture of ceramic and metal, subjected to statically mechanical and thermal loads [99]. Nonlinear free vibration of symmetric circular fiber-metal-laminated hybrid plates was published by Shooshtari and Dalir in 2015. In addition, Shooshtari and Dalir demonstrated the effects of several parameters on linear and nonlinear frequencies and the free vibration response on circular fiber-metal-laminated plates [100]. Afterwards, Ansari and Gholami considered the size effect by Eringen's nonlocal elasticity theory on the nonlinear first-order shear deformable beam model to carry out post-buckling analysis of magneto-electro-thermo-elastic nanobeams [101]. Rouzegar and Sharifpoor investigated the finite element formulations to carry out the free vibration analysis of isotropic and orthotropic plates using two-variable refined plate theory that predicts parabolic variations of transverse shear stresses along the thickness of the plate, satisfies the zero traction condition on the plate surfaces, and does not require the shear correction factor [102]. They demonstrated the effects of orthotropy ratio, side-to-thickness ratio, and types of boundary conditions on the natural frequencies of plates. Later, in 2017, Rafaeinejad et al. presented an analytical solution for bending, buckling, and free vibration of FG nanobeams [103]. Nanobeams were modeled resting on a double-parameter Winkler-Pasternak elastic foundation, and results were obtained using different nonlocal higher-order shear deformation beam theories. Rafaeinejad et al. showed clearly the effects of foundation, gradient index, aspect ratio, and nonlocal parameter on stability and vibration analysis. More recently, Jabbarian and Ahmadian conducted the free vibration analysis of a functionally graded stiffened micro-cylinder [104]. They took the size effect into consideration using the Modified Couple Stress Theory (MCST). Results demonstrated that the stiffeners yielded an increase in natural frequencies due to an increase in stiffness of the micro-cylinder. Further, in 2018, Sahoo et al. investigated the natural frequency and transient responses of carbon/epoxy layered composite plate structures by two higher-order mid-plane kinematic models [105].

In this paper, nanotubes and nanowires were modeled using classical Euler-Bernoulli beam theory (CT), Nonlocal Elasticity Theory (NET), Surface Elasticity Theory (SET), Modified Couple Stress Theory (MCST), Modified Strain Gradient Theory (MSGT), finite element model and COMSOL Multiphysics analysis software [106], and ANSYS software [107] to investigate critical and other buckling loads of simply supported boron nitride and silicon carbide nanotubes and nanowires. Comparative results are given in figures and tables.

The atomic structure of boron nitride and silicon carbide sheets is demonstrated in Figure 1. The top structure is the boron nitride sheet structure composed of hexagonally arranged boron (B) atoms and nitrogen N atoms. The bottom structure consists of silicon (Si) and carbon (C) atoms. In addition, the bond lengths of structures are demonstrated on the right side. Si-C bond length in silicene is 2.29 Å, where the B-N bond length is 1.42 Å in graphene; in this way, silicene can perform higher chemical reactivity than graphene, making silicene a weaker material than graphene.

As can be clearly seen from Figure 2, to obtain nanotubes, it is simply required to roll the nanosheet structured material. Nanostructures can be categorized into three main groups up to the angle they are rolled up. These three main groups are armchair, zigzag, and chiral [108].

To model nanotubes, classical Euler-Bernoulli beam theory is used with size-effective theories also by the hollow cylindrical beam model. Figure 3 shows transition from real BNNT (top) and SiCNT (middle) to its continuum mechanic model (bottom). Geometric parameters are also represented in Figure 3. A comparative image of BNNW and SiCNW is demonstrated in Figure 4. Furthermore, to model nanowires, the cylindrical beam model is used. Similarly, to demonstrate transition from nanowire to cylindrical beam model, Figure 5 depicts the geometric parameters. As observed, L and D represent the length and the diameter of nanowire, respectively.

In the current paper, nanostructures are analyzed for both with and without the elastic foundation

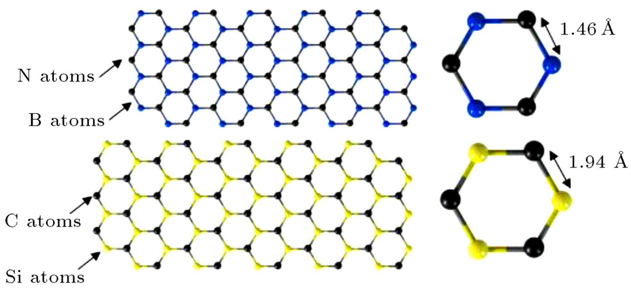

Figure 1. Atomic structure of boron nitride and silicon carbide sheets.

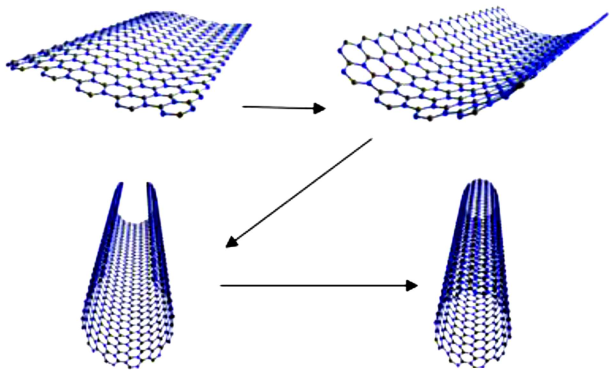

Figure 2. Transition from sheet structure to nanotube structure.

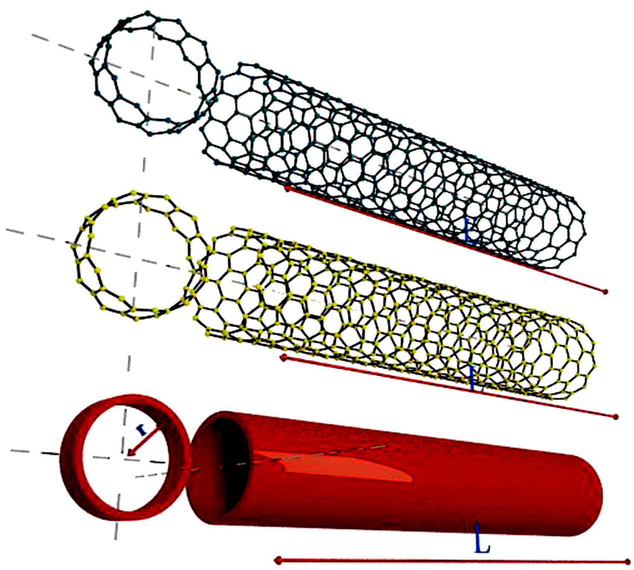

Figure 3. Demonstration of real and continuum models of nanotubes with geometric parameters.

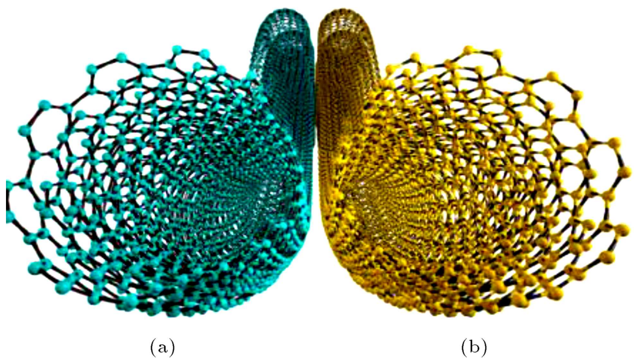

Figure 4. Structures of nanowires: (a) BNNW and (b) SiCNW.

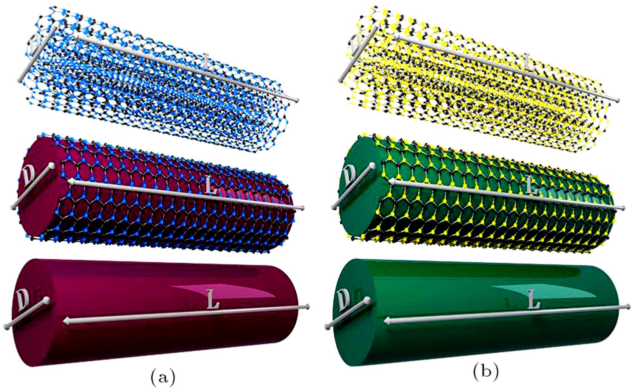

Figure 5. Transition from the real nanowire to its continuum model: (a) BNNT and (b) SiCNT.

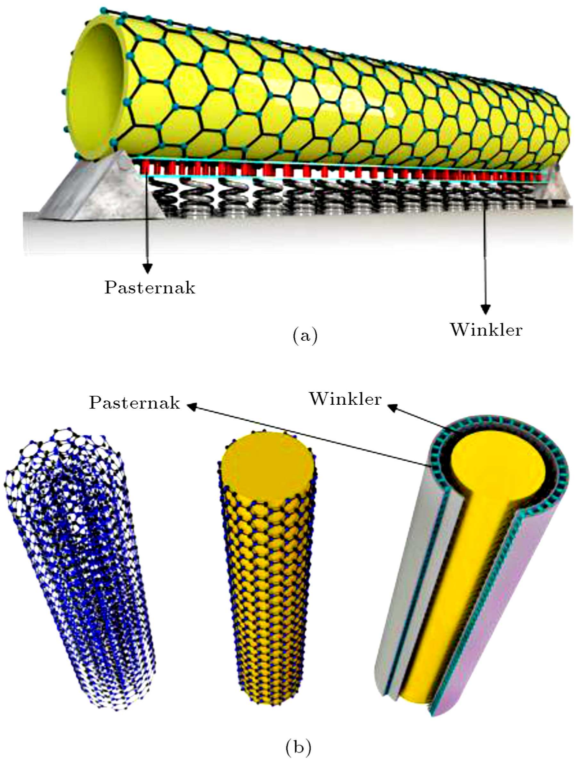

Figure 6. Continuum models of nanostructures on elastic foundation: (a) BNNT and (b) BNNW.

effect. Images of the continuum models on the double-parameter elastic foundation are shown in Figure 6 for nanotubes and nanowires. The Winkler foundation is attributed to springs in terms of its behavior, while the Pasternak foundation is demonstrated as vertical rods.

3. Formulations

3.1. *Modified couple stress and modified strain gradient theory*

The total deformation (strain) energy, U, based on MSGT can be written as follows [81]:

$$U=\frac{1}{2}\int_0^L\int_A(\sigma_{ij}\varepsilon_{ij}+p_i\gamma_i+\tau^{(1)}_{ijk}\eta^{(1)}_{ijk}+m^s_{ij}\chi^s_{ij})dAdx, \quad (1)$$

$$\varepsilon_{ij}=\frac{1}{2}(u_{i,j}+u_{j,i}), \quad (2)$$

$$\gamma_i=\varepsilon_{mm,i}, \quad (3)$$

$$\eta^{(1)}_{ijk}=\frac{1}{3}(\varepsilon_{jk,i}+\varepsilon_{ki,j}+\varepsilon_{ij,k}) -\frac{1}{15}\Big[\delta_{ij}(\varepsilon_{mm,k}+2\varepsilon_{mk,m}) + \delta_{jk}(\varepsilon_{mm,i}+2\varepsilon_{mi,m})+\delta_{ki}(\varepsilon_{mm,j}+2\varepsilon_{mj,m})\Big], \quad (4)$$

$$\chi^s_{ij}=\frac{1}{2}(\theta_{i,j}+\theta_{j,i}), \quad (5)$$

$$\theta_i=\frac{1}{2}e_{ijk}u_{k,j}, \quad (6)$$

where the rotation vector is denoted by θ, the strain tensor ε, the dilatation gradient vector γ, the deviatoric stretch gradient tensor $\eta^{(1)}$, and the symmetric rotation gradient tensor χ^s. Furthermore, δ is Kronecker delta symbol, and e_{ijk} is the permutation symbol. On the other hand, the components of the classical stress tensor σ (combined with the strain tensor) and the higher-order stress tensors p, $\tau^{(1)}$, and m^s (combined with the higher-order deformation gradient tensors) can be expressed as follows:

$$\sigma_{i,j}=\lambda\varepsilon_{mm}\delta_{ij}+2G\varepsilon_{ij}, \quad (7)$$

$$p_i=2Gl_0^2\gamma_i, \quad (8)$$

$$\tau^{(1)}_{ijk}=2Gl_1^2\eta^{(1)}_{ijk}\tau^{(1)}_{ijk}, \quad (9)$$

$$m^s_{ij}=2Gl_2^2\chi^s_{ij}, \quad (10)$$

where l_0, l_1, l_2 are length-scale parameters corresponding to dilatation gradient, deviatoric stretch gradients, and rotation gradients, respectively. Furthermore, λ and G represent Lamé constants. These Lamé constants can be expressed as follows:

$$\lambda=\frac{E\nu}{(1+\nu)(1-2\nu)},$$

$$G=\frac{E}{2(1+\nu)}. \quad (11)$$

According to Euler-Bernoulli beam theory, displacement components can be expressed as follows:

$$u_1(x,z) = -z\frac{dw(x)}{dx},$$

$$u_2(x,z) = 0,$$

$$u_3(x,z) = w(x), \tag{12}$$

where u_1, $i = 1,2,3$ are x, y, and z components of the displacement vector, respectively. The transverse displacement is expressed by $w(x)$. By substituting Eq. (12) into Eq. (2), the non-zero strain component can be found as follows:

$$\varepsilon_{11} = -z\frac{d^2v}{dx^2}. \tag{13}$$

By using Eqs. (12) and (13) and substituting them into Eqs. (3)-(5), the non-zero higher-order gradients can be obtained as follows:

$$\gamma_1 = -z\frac{d^3w}{dx^3},$$

$$\gamma_3 = -\frac{d^2w}{dx^2}, \tag{14}$$

$$\eta_{111}^{(1)} = -\frac{2}{5}z\frac{d^3w}{dx^3}, \quad \eta_{113}^{(1)} = \eta_{131}^{(1)} = \eta_{311}^{(1)} = -\frac{4}{15}\frac{d^2w}{dx^2},$$

$$\eta_{122}^{(1)} = \eta_{133}^{(1)} = \eta_{212}^{(1)} = \eta_{221}^{(1)} = \eta_{313}^{(1)} = \eta_{331}^{(1)} = \frac{1}{5}z\frac{d^3w}{dx^3}, \tag{15}$$

$$\eta_{223}^{(1)} = \eta_{232}^{(1)} = \eta_{322}^{(1)} = \frac{1}{15}\frac{d^2w}{dx^2}, \qquad \eta_{333}^{(1)} = \frac{1}{5}\frac{d^2w}{dx^2},$$

$$\chi_{12}^s = \chi_{21}^s = -\frac{1}{2}\frac{d^2w}{dx^2}. \tag{16}$$

To obtain the non-zero components of classical stress tensor, Eq. (13) needs to be substituted into Eq. (7):

$$\sigma_{11} = -E\eta z\frac{d^2w}{dx^2},$$

$$\sigma_{22} = \sigma_{33} = -\frac{Ev}{(1+v)(1-2v)}z\frac{d^2w}{dx^2}, \tag{17}$$

where:

$$\eta = \frac{(1-v)}{(1+v)(1-2v)}. \tag{18}$$

By using the above equations and substituting them into Eqs. (8)-(10), the non-zero components of higher-order stress tensors can be found as follows:

$$p_1 = -2Gl_0^2z\frac{d^3w}{dx^3}, \qquad p_3 = -2Gl_0^2\frac{d^2w}{dx^2}, \tag{19}$$

$$\tau_{111}^{(1)} = -\frac{4}{5}Gl_1^2z\frac{d^3w}{dx^3},$$

$$\tau_{113}^{(1)} = \tau_{131}^{(1)} = \tau_{311}^{(1)} = -\frac{8}{15}Gl_1^2\frac{d^2w}{dx^2},$$

$$\tau_{122}^{(1)} = \tau_{133}^{(1)} = \tau_{212}^{(1)} = \tau_{221}^{(1)} = \tau_{313}^{(1)} = \tau_{331}^{(1)}$$

$$= \frac{2}{5}Gl_1^2z\frac{d^3w}{dx^3}, \tag{20}$$

$$\tau_{223}^{(1)} = \tau_{232}^{(1)} = \tau_{322}^{(1)} = \frac{2}{15}Gl_1^2\frac{d^2w}{dx^2},$$

$$\tau_{333}^{(1)} = \frac{2}{5}Gl_1^2\frac{d^2w}{dx^2},$$

$$m_{12}^s = m_{21}^s = -Gl_2^2\frac{d^2w}{dx^2}. \tag{21}$$

Governing equations can be obtained by using the minimum total potential energy principle. According to the minimum total potential energy principle,

$$\delta\prod = \delta U - \delta W = 0, \tag{22}$$

where Π is the total potential energy. Furthermore, the first variation of strain energy and the work done by external forces are denoted by δU and δW, respectively. The first variation of the strain energy, δU, can be expressed as follows:

$$\delta U = \int_0^L\int_A (\sigma_{ij}\delta\varepsilon_{ij} + p\delta\gamma_i + \tau_{ijk}^{(1)}\delta\eta_{ijk}^{(1)} + m_{ij}^s\delta\eta_{ijk}^{(1)}$$

$$+ m_{ij}^s\delta\chi_{ijk}^s)dAdx = \int_0^L\Bigg[\Bigg(\Bigg(EI + GA(2l_0^2$$

$$+\frac{8}{15}l_1^2+l_2^2)\Bigg)\frac{d^4w}{dx^4} - 2GI\left(l_0^2+\frac{2}{5}l_1^2\right)\frac{d^6w}{dx^6}\Bigg)\delta w\Bigg]dx$$

$$+\int_0^L\Bigg[\Bigg(-(EI + GA(2l_0^2 + \frac{8}{15}l_1^2 + l_2^2))\frac{d^3w}{dx^3}$$

$$+ 2GI(l_0^2 + \frac{2}{5}l_1^2)\frac{d^5w}{dx^5}\Bigg)\delta w + \Bigg((EI$$

$$+ GA\left(2l_0^2 + \frac{8}{15}l_1^2 + l_2^2\right))\frac{d^2w}{dx^2}$$

$$- 2GI\left(l_0^2 + \frac{2}{5}l_1^2\right)\frac{d^4w}{dx^4}\Bigg)\delta\left(\frac{dw}{dx}\right)$$

$$+ 2GI\left(l_0^2 + \frac{2}{5}l_1^2\right)\frac{d^3w}{dx^3}\delta\left(\frac{d^2w}{dx^2}\right)\Bigg]_0^L. \tag{23}$$

The first variation of the work done by external forces can be expressed as follows:

$$\delta W = \int_0^L -\left(k_w w + (P-k_p)\frac{dw^2}{dx^2}\right)\delta w dx + \left[\left(V + (P-k_p)\frac{dw}{dx}\right)\delta w - M\delta\left(\frac{dw}{dx}\right) - M^{\eta c}\delta\left(\frac{dw^2}{dx^2}\right)\right]_0^L, \tag{24}$$

where the axial compressive force is denoted by P. Likewise, the shear force and classical and non-classical bending moments are represented with V, M, and M^{nc}, respectively. Winkler modulus and Pasternak modulus of the double-parameter elastic foundation are considered as k_w and k_p, respectively. By substituting Eqs. (24) and (26) into Eq. (23) (by setting $\delta w = 0$), the equilibrium equations for a Euler-Bernoulli beam can be obtained as follows:

$$\delta w \ : \ \left(EI + GA\left(2l_0^2 + \frac{8}{15}l_1^2 + l_2^2\right)\right)\frac{d^4 w}{dx^4} - 2GI\left(l_0^2 + \frac{2}{5}l_1^2\right)\frac{d^6 w}{dx^6} + (P-k_p)\frac{d^2 w}{dx^2} = 0. \tag{25}$$

To solve Eq. (25), boundary conditions need to be implemented. Simply supported boundary conditions placed at $x=0$ and $x=L$ can be expressed as follows:

$$\left(EI + GA\left(l_0^2 + \frac{8}{15}l_1^2 + l_2^2\right)\right)\frac{d^3 w}{dx^3} - 2GI\left(l_0^2 + \frac{2}{5}l_1^2\right)\frac{d^5 w}{dx^5} + V + (p-k_p)\frac{dw}{dx} = 0, \tag{26}$$

or $\delta w = 0$,

$$-(EI + GA(l_0^2 + \frac{8}{15}l_1^2 + l_2^2))\frac{d^2 w}{dx^2} + 2GI(l_0^2 + \frac{2}{5}l_1^2)\frac{d^4 w}{dx^4} = M$$

$$\text{or} \quad \delta\left(\frac{dw}{dx}\right) = 0, \tag{27}$$

$$-2GI(l_0^2 + \frac{2}{5}l_1^2)\frac{d^3 w}{dx^3} = M^{\eta c}$$

$$\text{or} \quad \delta\left(\frac{d^2 w}{dx^2}\right) = 0. \tag{28}$$

By applying Eqs. (26)-(28), the boundary conditions (classical and possible non-classical) can be considered as follows:

$$w = 0, \quad M = 0, \quad w'' = 0, \tag{29}$$

where:

$$w'' = \frac{d^2 w}{dx^2}. \tag{30}$$

In the case of simply supported boundary conditions:

$$B.w^{(4)} - D.w^{(6)} + Nw'' = 0. \tag{31}$$

The solution of Eq. (31) can be expressed as follows:

$$w(x) = C_1 + C_2 x + C_3 \sin Kx + C_4 \cos Kx + C_5 \sinh Mx + C_6 \cosh Mx, \tag{32}$$

where:

$$K = \left(\frac{-B + \sqrt{B^2 + 4DN}}{2D}\right)^{1/2},$$

$$M = \left(\frac{B + \sqrt{B^2 + 4DN}}{2D}\right)^{1/2}, \tag{33}$$

$C_i (i = 1, 2, ..., 6)$ are integral constants. These constants can be calculated by using boundary conditions. Substituting the boundary conditions of simply supported beams present in Eq. (29) and (30) into Eq. (32), we obtain the following:

$$C_i = 0 \quad \text{excluding} \quad C_3 \sin KL = 0. \tag{34}$$

The non-trivial solution to Eq. (34) can be considered as follows:

$$\sin KL = 0, \tag{35a}$$

$$K = \frac{n\pi}{L} \quad (n = 1, 2, ...), \quad N_{cr} = \frac{\pi^2}{L^2}\left(B + \frac{\pi^2 D}{L^2}\right). \tag{35b}$$

To solve Eq. (36), Navier's solution procedure can be applied as follows:

$$w(x) = \sum_{n=1}^{\infty} W_n \sin\left(\frac{n\pi x}{L}\right). \tag{36}$$

By using Navier's solution, the critical buckling loads for the simply supported nanowire on the double-parameter elastic foundation can be expressed as follows:

For MSGT:

$$P_{(n)} = \frac{n^2\pi^2}{L^2}\left[\left(EI + GA\left(2l_0^2 + \frac{8}{15}l_1^2 + l_2^2\right)\right) + \frac{n^2\pi^2}{L^2}\left(2GI\left(l_0^2 + \frac{2}{5}l_1^2\right)\right)\right] + k_w\frac{L^2}{n^2\pi^2} + k_p, \tag{37a}$$

For MCST:

$$P_{(n)} = \frac{n^2\pi^2}{L^2}\left[\,(EI + GA(l_2^2))\,\right] + k_w\frac{L^2}{n^2\pi^2} + k_p. \tag{37b}$$

3.2. Nonlocal Elasticity Theory (NET)

According to Eringen [89], the constitutive equation of Nonlocal Elasticity Theory (NET) can be expressed as follows:

$$[1-(e_0a)^2\nabla^2]\sigma_{ij} = C_{ijkl}, \tag{38}$$

where σ_{ij} is the nonlocal tensile tensor, $C_{ijkl}(x')$ is the local or classical tensile tensor at any x' point, a is a constant related to the characteristics of each material, and e_0 is the nonlocal parameter chosen within a range for each material.

The displacement of a thin beam (Euler-Bernoulli) can be expressed as follows:

$$u_1(x,z) = -z\frac{dw(x)}{dx},$$

$$u_2(x,z) = 0, \tag{39}$$

$$u_3(x,z) = w(x),$$

where u_1, u_2, u_3 are the x, y, z components of the displacement vector, and w represents the transverse displacement of the beam. According to thin beam theory, the relation between stress and displacement can be expressed as follows:

$$\varepsilon_{11} = \frac{du}{dx} = -z\frac{d^2w}{dx^2},$$

$$\varepsilon_{22} = \varepsilon_{33} = \varepsilon_{12} = \varepsilon_{13} = \varepsilon_{23} = 0, \tag{40}$$

where ε_{11} is the axial stress. In addition, the stress-strain equation according to thin beam theory can be expressed as follows:

$$\sigma_{11} = -Ez\frac{d^2w}{dx^2},$$

$$\sigma_{22} = \sigma_{33} = \tau_{12} = \tau_{13} = \tau_{23} = 0. \tag{41}$$

According to Eq. (38), the nonlocal stress-strain equation can be expressed as follows:

$$\sigma_{11} - \mu\frac{d^2\sigma_{11}}{dx^2} = E\varepsilon_{11}, \quad \mu = (e_0a)^2, \quad \sigma_{22} = 0$$

$$\sigma_{33} = 0 \quad \tau_{12} = \tau_{21} = 0, \quad \tau_{13} = \tau_{31} = 0,$$

$$\tau_{23} = \tau_{32} = 0. \tag{42}$$

To obtain governing equations, the minimum total energy principle is used. According to the minimum total energy principle:

$$\delta\prod = \delta U - \delta W = 0, \tag{43}$$

where Π denotes the total potential energy, and δU and δW are the first variation of stress and total energy from external loads, respectively. According to thin beam theory, δU and δW can be expressed as follows:

$$\delta U = \int_0^L\int_A(\sigma_{11}\delta\varepsilon_{11})\,dAdx = \int_0^L\int_A\left(\sigma_{11}\left(-z\frac{d^2\delta w}{dx^2}\right)\right)dAdx, \tag{44}$$

$$\delta W = \int_0^L\left(P\frac{dw}{dx}\delta\frac{dw}{dx} + qw(x)\right)dx. \tag{45}$$

Substituting Eqs. (44) and (45) into Eq. (43), we obtain:

$$\int_0^L\left(-M\frac{d^2\delta w}{dx^2}\right)dx - \int_0^L\left(P\frac{dw}{dx}\delta\frac{dw}{dx} + q\delta w(x)\right)dx = 0, \tag{46}$$

where P is the axial load.

By partially integrating Eq. (46), the buckling equation and boundary conditions can be obtained as follows:

$$\delta\mathrm{w}: \frac{dw}{dx}\left(P\frac{dw}{dx}\right) - q = \frac{d^2M}{dx^2}, \tag{47}$$

$$\frac{dM}{dx} - P\frac{dw}{dx} = 0, \quad M = 0. \tag{48}$$

The nonlocal moment can be written by using Eq. (42) as follows:

$$M - \mu\frac{d^2M}{dx^2} = -EI\frac{d^2w}{dx^2}. \tag{49}$$

By substituting Eq. (47) in Eq. (49), the nonlocal moment can be obtained as follows:

$$M = \mu\left(\frac{d}{dx}\left(P\frac{dw}{dx}\right) - q\right) - EI\frac{d^2w}{dx^2}. \tag{50}$$

Using the fourth-order derivative of nonlocal moment into Eq. (47), we obtain:

$$\delta\mathrm{w}: \frac{d^2}{dx^2}\left(-EI\frac{d^2w}{dx^2}\right) + \mu\frac{d^2}{dx^2}\left(\frac{d}{dx}\left(P\frac{dw}{dx}\right) - q\right) + q - \frac{d}{dx}\left(P\frac{dw}{dx}\right) = 0. \tag{51}$$

The nonlocal boundary conditions are as follows:

$$\frac{d}{dx}\left(\mu\left(\frac{d}{dx}\left(P\frac{dw}{dx}\right)-q\right)-EI\frac{d^2w}{dx^2}\right)-P\frac{dw}{dx}=0. \tag{52}$$

$$\mu\left(\frac{d}{dx}\left(P\frac{dw}{dx}\right)-q\right)-EI\frac{d^2w}{dx^2}=0.$$

The relation between load and elastic foundations can be established as follows:

$$p(x)=k_w w-k_p\frac{d^2w}{dx^2}. \tag{53}$$

Substituting Eq. (53) into Eq. (51) gives:

$$\left(-EI+P\mu-k_p\mu\right)\frac{d^4w}{dx^4}+\left(k_w\mu-P+k_p\right)\frac{d^2w}{dx^2}-k_w w=0. \tag{54}$$

In the case of simply supported nanobeams, the fundamental boundary conditions can be expressed as follows:

$$\delta\left[w\right]_0^L=0,\quad \delta\left[\frac{dw}{dx}\right]_0^L=0. \tag{55}$$

Natural boundary conditions are also expressed as follows:

$$\left[\left(-EI+P\mu-k_p\mu\right)\frac{d^2w}{dx^2}+\mu k_w w\right]_0^L,\quad \text{and}$$

$$\left[\left(-EI+P\mu-k_p\mu\right)\frac{d^3w}{dx^3}+\left(k_w\mu-P\right)\frac{dw}{dx}\right]_0^L. \tag{56}$$

The nonlocal buckling equation is given in Eq. (54). To simplify the equation, the expressions expressed below can be used:

$$A=-EI+P\mu-k_p\mu,$$

$$B=k_w\mu-P+k_p,$$

$$C=k_w. \tag{57}$$

A simplified version of Eq. (54) is obtained after implementing Eq. (57):

$$Aw^{iv}+Bw^{ii}-Cw=0. \tag{58}$$

To solve Eq. (58), it can be assumed that $w=e^{rx}$. Then, Eq. (58) can be expressed as follows:

$$Ar^4e^{rx}+Br^2e^{rx}-Ce^{rx}=0. \tag{59}$$

Roots of Eq. (59) are as follows:

$$r_{1,2}=\pm i\sqrt{\frac{B-\sqrt{B^2+4AC}}{2A}},$$

$$r_{3,4}=\pm\left[\sqrt{\frac{\sqrt{B^2+4AC}}{2A}-\frac{B}{2A}}\right], \tag{60}$$

$$\psi=\sqrt{\frac{B-\sqrt{B^2+4AC}}{2A}},$$

$$\zeta=\sqrt{\frac{\sqrt{B^2+4AC}}{2A}-\frac{B}{2A}}. \tag{61}$$

By substituting roots into Eq. (58) and solving it, we obtain:

$$w=C_1\sin\psi x+C_2\cos\psi x+C_3\cosh\zeta x+C_4\sinh\zeta x. \tag{62}$$

As stated before, C_1, C_2, C_3, and C_4 are those constants that can be found by using boundary conditions. The first derivative of Eq. (62) can be stated as follows:

$$w'=\psi C_1\cos\psi x-\psi C_2\sin\psi x+\zeta C_3\sinh\zeta x+\zeta C_4\cosh\zeta x. \tag{63}$$

The second derivative of Eq. (62) can be expressed by Eq. (64) as shown in Box I. Similarly, the third derivative of Eq. (62) can be expressed as follows:

$$V=-\left(\left(-k_we_0a^2+P\right)\left(\psi^2C_2\cos\psi x-\zeta^2C_3\cosh\zeta x+\psi^2C_1\sin\psi x-\zeta^2C_4\sinh\zeta x\right)-\psi C_1\cos\psi x+\zeta C_4\cosh\zeta x+\psi C_2 sin\psi x+\zeta C_3\sinh\zeta x\right)/\left(EI-Pe_0a^2+e_0a^2k_p\right). \tag{65}$$

Boundary conditions of a simply supported beam can be expressed as follows:

$$w(0)=M(0)=w(l)=M(l)=0. \tag{66}$$

By substituting Eq. (66) into Eqs. (64) and (65), the following equations can be obtained:

$$w(0)=C_2+C_3=0, \tag{67}$$

$$M(0)=-\psi^2-\frac{e_0a^2k_w}{EI-P*e_0a^2+e_0a^2*k_p}C_2+\zeta^2-\frac{e_0a^2k_w}{EI-P*e_0a^2+e_0a^2*k_p}C_3=0, \tag{68}$$

$$M=-\psi^2C_1\sin\psi x-\psi^2C_2\cos\psi x+\zeta^2C_3\cosh\zeta x+\zeta^2C_4\sinh\zeta x$$
$$-\frac{e_0a^2k_w(C_2\cos\psi x+C_3\cosh\zeta x+C_1\sin\psi x+C_4\sinh\zeta x)}{EI-Pe_0a^2+e_0a^2k_p}. \quad (64)$$

Box I

$$w(l)=C_1\sin\psi l+C_2\cos\psi l+C_3\cosh\zeta l$$
$$+C_4\sinh\zeta l=0, \quad (69)$$

$$M(l)=-C_1\left(\psi^2\sin\psi l+\frac{e_0a^2k_w\sin\psi l}{EI-P*e_0a^2+e_0a^2*k_p}\right)$$
$$-C_2\left(\psi^2\cos\psi l+\frac{e_0a^2k_w\cos\psi l}{EI-P*e_0a^2+e_0a^2*k_p}\right)$$
$$+C_3\left(\zeta^2\cosh\zeta l-\frac{e_0a^2k_w\cosh\zeta l}{EI-P*e_0a^2+e_0a^2*k_p}\right)$$
$$+C_4\left(\zeta^2\sinh\zeta l-\frac{e_0a^2k_w\sinh\zeta l}{EI-P*e_0a^2+e_0a^2*k_p}\right)$$
$$=0. \quad (70)$$

As stated before, C_1, C_2, C_3, and C_4 are those constants that can be determined through Eqs. (67)-(70). To solve these four equations with four unknown constants, Eqs. (67)-(70) can be written in the matrix form as follows:

$$\begin{bmatrix} 0 & 1 & 1 & 0 \\ 0 & -\psi^2+\frac{e_0a^2C}{A} & \zeta^2+\frac{e_0a^2C}{A} & 0 \\ \sin\psi l & \cos\psi l & \cosh\zeta l & \sinh\zeta l \\ \lambda_1 & \lambda_2 & \lambda_3 & \lambda_4 \end{bmatrix}$$
$$\begin{Bmatrix} C_1 \\ C_2 \\ C_3 \\ C_4 \end{Bmatrix}=0$$

$$\lambda_1=-\left(\psi^2\sin\psi l-\frac{e_0a^2C\sin\psi l}{A}\right),$$
$$\lambda_2=-\left(\psi^2\cos\psi l-\frac{e_0a^2C\cos\psi l}{A}\right),$$
$$\lambda_3=\left(\zeta^2\cosh\zeta l+\frac{e_0a^2C\cosh\zeta l}{A}\right),$$
$$\lambda_4=\left(\zeta^2\sinh\zeta l+\frac{e_0a^2k_w\sinh\zeta l}{A}\right). \quad (71)$$

Taking the determinant of the matrix given in Eq. (71), we obtain:

$$\sin\psi l\sinh\zeta l\left(\psi^2+\zeta^2\right)^2=0. \quad (72)$$

There are three possibilities to equalize Eq. (72). These three possibilities can be explored as follows:

$$\left(\psi^2+\zeta^2\right)^2=0, \quad (35)$$
$$\sin\psi l=0, \quad (74)$$
$$\sinh\zeta l=0. \quad (75)$$

The non-trivial solution can be found as follows:

$$\sin\psi l=0,\quad \psi l=n\pi,\quad n=0,1,2,... \quad (76)$$
$$\psi^2l^2=n^2\pi^2, \quad (77)$$
$$\frac{B-\sqrt{B^2+4AC}}{2A}l^2=n^2\pi^2. \quad (78)$$

By substituting the values of A, B, and C given in Eqs. (57) to (78), the final form of nonlocal buckling equation can be obtained:

$$P(n)=\frac{(\overline{EI}+k_p\mu)\left(\frac{n\pi}{L}\right)^4+(k_w\mu+k_p)\left(\frac{n\pi}{L}\right)^2+k_w}{\mu\left(\frac{n\pi}{L}\right)^4+\left(\frac{n\pi}{L}\right)^2}. \quad (79)$$

3.3. Surface Elasticity Theory (SET)

Gurtin and Murdoch have proposed the surface constitutive as follows [109,110]:

$$\tau_{11}=\tau_0+(2\mu_0+\lambda_0)u_{11},$$
$$\tau_{n1}=\tau_0u_{n,1}, \quad (80)$$

where Lamé constants are denoted by μ_0 and λ_0 and residual surface stress by τ_0. The displacement of a Timoshenko beam can be expressed as follows:

$$u_1=z\phi(x,t),$$
$$u_2=w(x,t), \quad (81)$$

where u_1 and u_2 are the components of the displacement vector, respectively, and w represents the transverse displacement of the beam. The relation between strain and displacement can be expressed as follows:

$$\varepsilon_1 = \frac{du_x}{dx} = -z\frac{d^2w}{dx^2},$$

$$\varepsilon_{22} = 0,$$

$$\varepsilon_{12} = \frac{1}{2}\left(\frac{du_x}{dx} + \frac{du_z}{dx}\right) = \frac{1}{2}\left(\frac{dw_{(x,t)}}{dx} + \phi_{(x,t)}\right). \tag{82}$$

To obtain surface stress field, Eq. (81) needs to be substituted into Eq. (80):

$$\tau_{11} = \tau_0 - z(2\mu_0 + \lambda_0)\frac{d^2w(x)}{dx^2},$$

$$\tau_{n1} = \tau_0\frac{dw(x)}{dx}n_2. \tag{83}$$

By using Eq. (83), the vertical stresses of both top and bottom surfaces of the layer can be obtained in the case of $n_2 = 1$:

Top layer:

$$\tau_{21} = \tau_0\frac{dw(x)}{dx},$$

Bottom layer:

$$\tau_{21} = -\tau_0\frac{dw(x)}{dx}. \tag{84}$$

By using Eqs. (84) and (81), the vertical stress can be obtained as follows:

$$\sigma_{22} = \frac{2z}{H}\tau_0\frac{d^2w(x)}{dx^2} - \rho_0\frac{d^2w}{dt^2}. \tag{85}$$

The non-zero bulk stresses can be expressed by using Eq. (85) as follows:

$$\sigma_{11} = E(z\frac{d\phi}{dx}) + \frac{2vz}{H}(\tau_0\frac{d^2w}{dx^2} - \rho_0\frac{d^2w}{dt^2}, \tag{86}$$

$$\sigma_{12} = GK(\frac{dw(x)}{dx} + \phi), \tag{87}$$

$$\sigma_{22} = \frac{2z}{H}(\tau_0\frac{d^2w(x)}{dx^2} - \rho_0\frac{d^2w}{dt^2}). \tag{88}$$

In Eq. (87), K represents the shear correction coefficient, which is neglected for Euler-Bernoulli beams. The stress field of the beam can be found by Eqs. (86)-(88) and (83). Consequently, the governing equation including surface effect for a Timoshenko beam can be expressed as follows:

$$GKA\left(\frac{d^2w(x)}{dx^2} + \frac{d\phi}{dx}\right) + \tau_0 s^*\frac{d^2w}{dx^2} - q(x) = (\rho A + \rho_0 s^*)\frac{d^2w}{dt^2}, \tag{89}$$

$$(EI + (2\mu_0 + \lambda_0)I^*)\frac{d^2\phi}{dx^2} + \frac{2vI\tau_0}{H}\frac{d^3w}{dx^3} - GKA\left(\frac{dw(x)}{dx} + \phi\right) = (\rho A + \rho_0 s^*)\frac{d^2w}{dt^2}, \tag{90}$$

where I^* represents the perimeter moment of inertia, and s^* is calculated by the following equation:

$$s^* = \int_s n_2^2 ds. \tag{91}$$

To calculate these values for ZnO nanowire with circular cross-section, the following are used:

$$H = 2\tau_0 D, \tag{92}$$

$$s^* = \frac{\pi D}{2}, \tag{93}$$

$$I^* = \frac{\pi D^3}{8}. \tag{94}$$

To obtain the governing equation for a Euler-Bernoulli beam, the rotational inertia needs to be ignored in Eq. (90) as follows:

$$GKA\left(\frac{dw(x)}{dx} + \phi\right) = (EI + (2\mu_0 + \lambda_0)I^*)\frac{d^2\phi}{dx^2}, + \frac{2vI\tau_0}{H}\frac{d^3w}{dx^3} - \frac{2vI\rho_0}{H}\frac{d^3w}{dxdt}. \tag{95}$$

By taking the first derivative of Eq. (95) and using Eq. (89), we obtain:

$$\left(EI + (2\mu_0 + \lambda_0)I^* - \frac{2vI\tau_0}{H}\right)\frac{d^4w}{dx^4} - \tau_0 s^*\frac{d^2w}{dx^2} + q(x) = -(\rho A + \rho_0 s^*)\frac{d^2w}{dx^2} - \frac{2vI\rho_0}{H}\frac{d^4w}{dx^2dt^2}, \tag{96}$$

By simplifying Eq. (96), we obtain:

$$\left(EI + (2\mu_0 + \lambda_0)I^* - \frac{2vI\tau_0}{H}\right)\frac{d^4w}{dx^4} + P - \tau_0 s^*\frac{d^2w}{dx^2} + q(x) = 0, \tag{97}$$

where:

$$q(x) = H\frac{d^2w}{dx^2} - k_w w + k_p\frac{d^2w}{dx^2}. \quad (98)$$

The general solution of Eq. (97) can be obtained through the following equation:

$$w(x) = C_1\cos\beta x + C_2\sin\beta x + C_3x + C_4 + w_q(x), \quad (99)$$

where:

$$\beta = \sqrt{\frac{P - \tau_0 s^*}{EI + (2\mu_0+\lambda_0)I^* - \frac{2vI\tau_0}{H}}}. \quad (100)$$

In addition, C_1, C_2, C_3, and C_4 need to be calculated by using boundary conditions. By substituting the boundary conditions given in Eq. (66), we obtain:

$$C_1 + C_4 = 0,$$

$$-\beta^2 C_1 = 0,$$

$$C_1\cos\beta L + C_2\sin\beta L + C_3L + C_4 = 0,$$

$$-C_1\beta^2\cos\beta L - C_2\beta^2\sin\beta L = 0. \quad (101)$$

By solving the above equations, the buckling formulation of Euler-Bernoulli beam including surface effect on the double-parameter elastic foundation can be obtained as follows:

$$P(n) = \frac{\overline{EI}\left(\frac{n\pi}{L}\right)^4 + (H+k_p)\left(\frac{n\pi}{L}\right)^2 k_w}{\left(\frac{n\pi}{L}\right)^2}, \quad (102)$$

where $\overline{EI}$ is the flexural rigidity and can be calculated as follows:

$$\overline{EI} = EI + EI^*. \quad (103)$$

3.4. Finite element model

The stiffness matrix obtained by bending effect can be expressed as follows:

$$K = \int_{t_1}^{t_2}\int_0^L EI^{\phi''^T\phi''} u\,dxdt,$$

$$K_{wy} = \int_{t_1}^{t_2}\int_0^L k_w{}^{\phi^T\phi}dxdt,$$

$$K_{wyo} = \int_{t_1}^{t_2}\int_0^L (e_0a)^2 k_w{}^{\phi'^T\phi'}dxdt,$$

$$K_{py} = \int_{t_1}^{t_2}\int_0^L k_p{}^{\phi'^T\phi'}dxdt,$$

$$K_{pyo} = \int_{t_1}^{t_2}\int_0^L (e_0a)^2 k_p{}^{\phi''^T\phi''}dxdt, \quad (104)$$

$$K_{gy} = \int_{t_1}^{t_2}\int_0^L P^{\phi'^T\phi'}dxdt,$$

$$K_{gyo} = \int_{t_1}^{t_2}\int_0^L (e_0a)^2 P^{\phi''^T\phi''}dxdt,$$

$$F_y = \int_{t_1}^{t_2}\int_0^L q^{\phi^T}dxdt,$$

$$F_{yo} = \int_{t_1}^{t_2}\int_0^L (e_0a)^2 q^{\phi''^T}dxdt.$$

By applying nondimensional shape functions :

$$K = K_e = \int_0^1 \left[EI\frac{1}{L^4}\frac{\partial^2\phi^T}{\partial\xi^2}\frac{\partial^2\phi}{\partial\xi^2}L\partial\xi\right]$$

$$= \int_0^1 \frac{EI}{L^3}\begin{Bmatrix}\phi_1''\\ \phi_2''\\ \phi_3''\\ \phi_4''\end{Bmatrix}\begin{bmatrix}\phi_1'' & \phi_2'' & \phi_3'' & \phi_4''\end{bmatrix}d\xi$$

$$= \int_0^1 \frac{EI}{L^3}\begin{bmatrix}\phi_1''\phi_1'' & \phi_1''\phi_2'' & \phi_1''\phi_3'' & \phi_1''\phi''\\ \phi_2''\phi_1'' & \phi_2''\phi_2'' & \phi_2''\phi_3'' & \phi_2''\phi''\\ \phi_3''\phi_1'' & \phi_3''\phi_2'' & \phi_3''\phi_3'' & \phi_3''\phi''\\ \phi_4''\phi_1'' & \phi_4''\phi_2'' & \phi_4''\phi_3'' & \phi_4''\phi''\end{bmatrix}d\xi,$$

$$K_e = \frac{EI}{L^3}\begin{bmatrix}12 & 6L & -12 & 6L\\ 6L & 4L^2 & -6L & 2L^2\\ -12 & -6L & 12 & -6L\\ 6L & 2L^2 & -6L & 4L^2\end{bmatrix}. \quad (105)$$

Similarly, the effect of Winkler foundation can be expressed as follows [111]:

$$K_w = K_{wy} + K_{wyo} = \int_0^1 \left[k_w\phi^T\phi L\partial\xi\right]$$

$$+ \int_0^1 \left[(e_0a)^2\frac{1}{L^2}k_w\frac{\partial\phi^T}{\partial\xi}\frac{\partial\phi}{\partial\xi}L\partial\xi\right]$$

$$= \int_0^1 k_w L \begin{bmatrix} \phi_1\phi_1 & \phi_1\phi_2 & \phi_1\phi_3 & \phi_1\phi_4 \\ \phi_2\phi_1 & \phi_2\phi_2 & \phi_2\phi_3 & \phi_2\phi_4 \\ \phi_3\phi_1 & \phi_3\phi_2 & \phi_3\phi_3 & \phi_3\phi_4 \\ \phi_4\phi_1 & \phi_4\phi_2 & \phi_4\phi_3 & \phi_4\phi_4 \end{bmatrix} \partial\xi$$

$$+ \int_0^1 \frac{(e_0a)^2 k_w}{L}$$

$$\begin{bmatrix} \phi_1'\phi_1' & \phi_1'\phi_2' & \phi_1'\phi_3' & \phi_1'\phi_4' \\ \phi_2'\phi_1' & \phi_2'\phi_2' & \phi_2'\phi_3' & \phi_2'\phi_4' \\ \phi_3'\phi_1' & \phi_3'\phi_2' & \phi_3'\phi_3' & \phi_3'\phi_4' \\ \phi_4'\phi_1' & \phi_4'\phi_2' & \phi_4'\phi_3' & \phi_4'\phi_4' \end{bmatrix} \partial\xi. \tag{106}$$

$$K_w = \frac{k_w}{420} \begin{bmatrix} 156L & 22L^2 & 54L & -13L^2 \\ 22L^2 & 4L^3 & 13L^2 & -3L^3 \\ 54L & 13L^2 & 156L & -22L^2 \\ -13L^2 & -3L^3 & -22L^2 & 4L^3 \end{bmatrix}$$

$$+ \frac{(e_0a)^2 k_w}{30L} \begin{bmatrix} 36 & 3L & -36 & 3L \\ 3L & 4L^2 & -3L & -L^2 \\ -36 & -3L & 36 & -3L \\ 3L & -L^2 & -3L & 4L^2 \end{bmatrix}.$$

The matrix form of the Pasternak foundation can be expressed as follows:

$$K_k = K_{py} + K_{pyo} = \int_0^1 \left[\frac{1}{L^2} k_p \frac{\partial\phi^T}{\partial\xi}\frac{\partial\phi}{\partial\xi} L\partial\xi\right]$$

$$+ \int_0^1 \left[\frac{(e_0a)^2 k_p}{L^4}\frac{\partial^2\phi^T}{\partial\xi^2}\frac{\partial^2\phi}{\partial\xi^2} L\partial\xi\right]$$

$$= \int_0^1 \frac{k_p}{L} \begin{bmatrix} \phi_1'\phi_1' & \phi_1'\phi_2' & \phi_1'\phi_3' & \phi_1'\phi_4' \\ \phi_2'\phi_1' & \phi_2'\phi_2' & \phi_2'\phi_3' & \phi_2'\phi_4' \\ \phi_3'\phi_1' & \phi_3'\phi_2' & \phi_3'\phi_3' & \phi_3'\phi_4' \\ \phi_4'\phi_1' & \phi_4'\phi_2' & \phi_4'\phi_3' & \phi_4'\phi_4' \end{bmatrix} \partial\xi$$

$$+ \int_0^1 \frac{(e_0a)^2 k_p}{L^3}$$

$$\begin{bmatrix} \phi_1''\phi_1'' & \phi_1''\phi_2'' & \phi_1''\phi_3'' & \phi_1''\phi_4'' \\ \phi_2''\phi_1'' & \phi_2''\phi_2'' & \phi_2''\phi_3'' & \phi_2''\phi_4'' \\ \phi_3''\phi_1'' & \phi_3''\phi_2'' & \phi_3''\phi_3'' & \phi_3''\phi_4'' \\ \phi_4''\phi_1'' & \phi_4''\phi_2'' & \phi_4''\phi_3'' & \phi_4''\phi_4'' \end{bmatrix} \partial\xi,$$

$$K_k = \frac{k_p}{30L} \begin{bmatrix} 36 & 3L & -36 & 3L \\ 3L & 4L^2 & -3L & -L^2 \\ -36 & -3L & 36 & -3L \\ 3L & -L^2 & -3L & 4L^2 \end{bmatrix}$$

$$+ (e_0a)^2 \frac{k_p}{L^3} \begin{bmatrix} 12 & 6L & -12 & 6L \\ 6L & 4L^2 & -6L & 2L^2 \\ -12 & -6L & 12 & -6L \\ 6L & 2L^2 & -6L & 4L^2 \end{bmatrix}. \tag{107}$$

The matrix caused by axial load:

$$K_g = K_{gy} + K_{gyo} = \int_0^1 \left[\frac{1}{L^2} P \frac{\partial\phi^T}{\partial\xi}\frac{\partial\phi}{\partial\xi} L\partial\xi\right]$$

$$+ \int_0^1 \left[\frac{(e_0a)^2 P}{L^4}\frac{\partial^2\phi^T}{\partial\xi^2}\frac{\partial^2\phi}{\partial\xi^2} L\partial\xi\right]$$

$$= \int_0^1 \frac{P}{L} \begin{bmatrix} \phi_1'\phi_1' & \phi_1'\phi_2' & \phi_1'\phi_3' & \phi_1'\phi_4' \\ \phi_2'\phi_1' & \phi_2'\phi_2' & \phi_2'\phi_3' & \phi_2'\phi_4' \\ \phi_3'\phi_1' & \phi_3'\phi_2' & \phi_3'\phi_3' & \phi_3'\phi_4' \\ \phi_4'\phi_1' & \phi_4'\phi_2' & \phi_4'\phi_3' & \phi_4'\phi_4' \end{bmatrix} \partial\xi$$

$$+ \int_0^1 \frac{(e_0a)^2 P}{L^3}$$

$$\begin{bmatrix} \phi_1''\phi_1'' & \phi_1''\phi_2'' & \phi_1''\phi_3'' & \phi_1''\phi_4'' \\ \phi_2''\phi_1'' & \phi_2''\phi_2'' & \phi_2''\phi_3'' & \phi_2''\phi_4'' \\ \phi_3''\phi_1'' & \phi_3''\phi_2'' & \phi_3''\phi_3'' & \phi_3''\phi_4'' \\ \phi_4''\phi_1'' & \phi_4''\phi_2'' & \phi_4''\phi_3'' & \phi_4''\phi_4'' \end{bmatrix} \partial\xi,$$

$$K_g = \frac{P}{30L} \begin{bmatrix} 36 & 3L & -36 & 3L \\ 3L & 4L^2 & -3L & -L^2 \\ -36 & -3L & 36 & -3L \\ 3L & -L^2 & -3L & 4L^2 \end{bmatrix}$$

$$+ (e_0a)^2 \frac{P}{L^3} \begin{bmatrix} 12 & 6L & -12 & 6L \\ 6L & 4L^2 & -6L & 2L^2 \\ -12 & -6L & 12 & -6L \\ 6L & 2L^2 & -6L & 4L^2 \end{bmatrix}. \tag{108}$$

In Figure 7, the solving method in finite element is plotted. Basically, finite element analysis slices an object into numerous pieces and, then, connects the intersections.

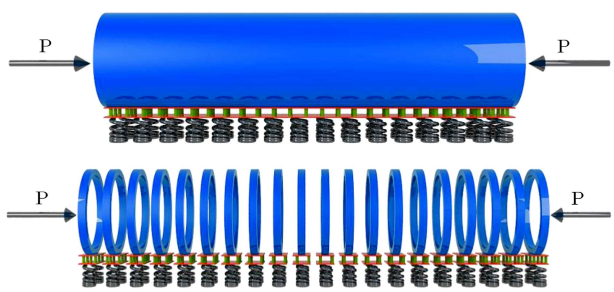

Figure 7. Demonstration of finite element method slicing.

To obtain the results, the following eigenvalue problem needs to be solved:

$$|K - \lambda K_g| = 0. \tag{109}$$

The stiffness matrix is:

$$[K] = [K_e] + [K_w] + [K_k]. \tag{110}$$

If the axial load is any compression load, then:

$$K_g = [K_g]. \tag{111}$$

4. Numerical results and discussion

The stability analysis of silicon carbide and boron nitride nanotubes and nanowires resting on an elastic substrate was carried out in the present study. To model the nanostructures, Euler-Bernoulli beam theory was employed. Since the analysis was done on a nano scale, different small-scale effective theories were used to take small-scale effect into consideration. Nonlocal elasticity theory, surface elasticity theory and its combination with the former theory, modified strain gradient theory, and modified couple stress theories were used and compared to investigate their influence on the buckling results. In addition, finite element analysis was applied to nanostructures both by the continuum model and computer software products. In figures, nonlocal elasticity theory is represented as NET, surface elasticity theory as SET, the combination of nonlocal elasticity theory and surface elasticity theory as NSET, modified strain gradient theory as MSGT, and modified couple stress theory as MCST. To obtain dimensionless analysis results, Winkler and Pasternak foundation parameters are used in the dimensionless form as $K_w = \frac{k_w L^4}{EI}$ and $K_p = \frac{k_p L^2}{EI}$, respectively.

In Figure 8, the mode shape of nanostructures is plotted by ANSYS computer software. Parameters of

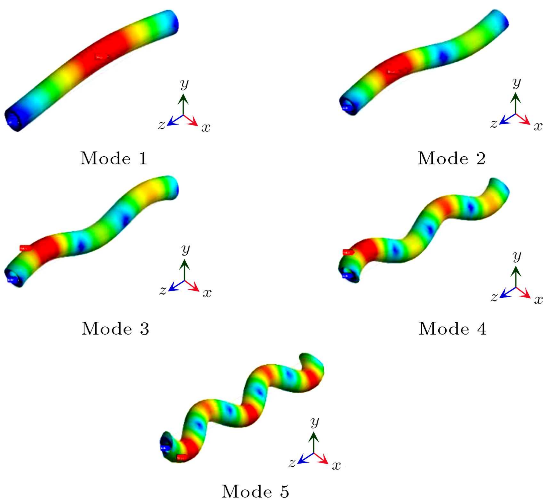

Figure 8. Buckling analysis mode shapes (ANSYS).

size-effective theories were selected as follows: $E^s = 35.3$, $\mu = 4$ nm, $l_0 = l_1 = l_2 = 0.5$ [46]. The effect of Winkler parameter was investigated for all size-effective theories, as shown in Figure 9. The dimensionless buckling loads were calculated with a change in the Winkler foundation parameter. For the calculation shown in Figure 9, the effect of Pasternak foundation was neglected by setting the value of the Pasternak foundation parameter to zero.

As observed clearly from Figure 9, the effect of Winkler foundation gets dramatically lower on higher modes. It can also be observed that the nonlocal elasticity theory lowers buckling load due to the fragile nanostructure, while modified couple stress theory, modified strain gradient theory, and surface elasticity theory produce higher results by strengthening the nanostructure. Between size-effective theories, modified strain gradient theory always yields the highest results, while the nonlocal elasticity theory yields the lowest results for all modes.

The dimensionless buckling loads were calculated with a change in Pasternak foundation parameter in Figure 10. The effect of Winkler foundation was neglected by setting the value of the Winkler foundation parameter to zero. Similar to previous results, the effect of the foundation gets lower, yet not as low as that of Winkler foundation.

In Table 1, critical buckling loads of nanostructures are calculated and compared. To validate the results, the comparison of the results with those of Naidu and Rao [112] is made, and they appear to be in good harmony. In Table 1, N represents the element number used for finite element analysis. Finite element method results are both given for various nonlocal elasticity parameters and classic analysis. Similar to Figures 9 and 10, the lowest results are obtained for the highest nonlocal parameter ($e_0 a = 10$ nm). Choosing a higher value of the size-effective parameter for MCST and MSGT ends with a higher buckling load value.

5. Concluding remarks

The effect of the double-parameter elastic foundation on buckling of silicon carbide and boron nitride nanotubes and nanowires was investigated in the current study. To model the nanostructures, Euler-Bernoulli beam model and computer software products were used. Since the beams were of nano-size to consider small scales, three different small-scale effect theories were used, whose results were compared with finite element results. Small-scale effective theories used include nonlocal elasticity theory, surface elasticity theory and their combination, modified strain gradient theory, and modified couple stress theory. The substrate was modeled by using the two-parameter (Winkler and Pasternak) elastic foundation model. Buckling loads

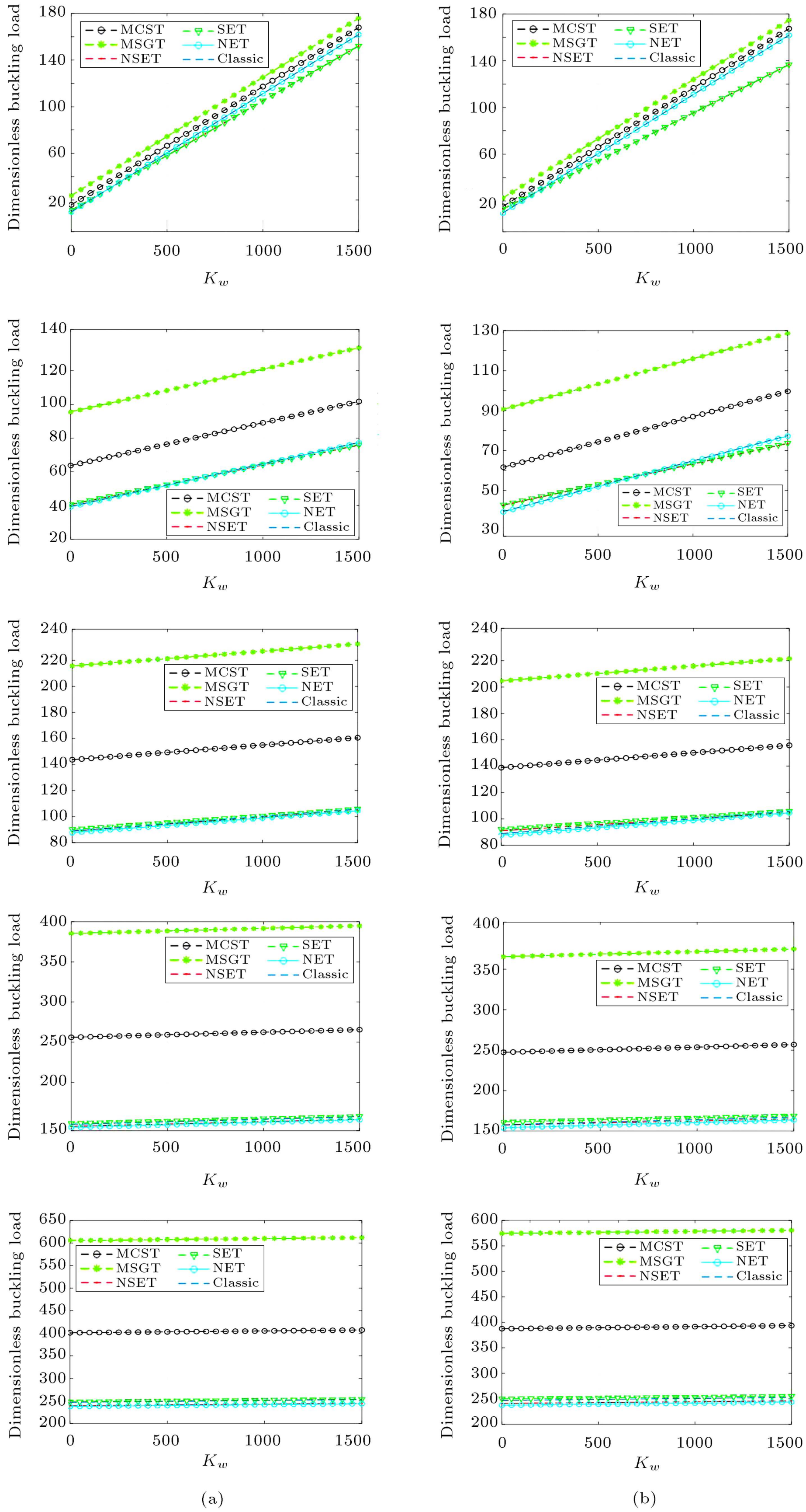

Figure 9. Buckling analysis results with a change in Winkler foundation for the first five modes: (a) BNNT and (b) SiCNT.

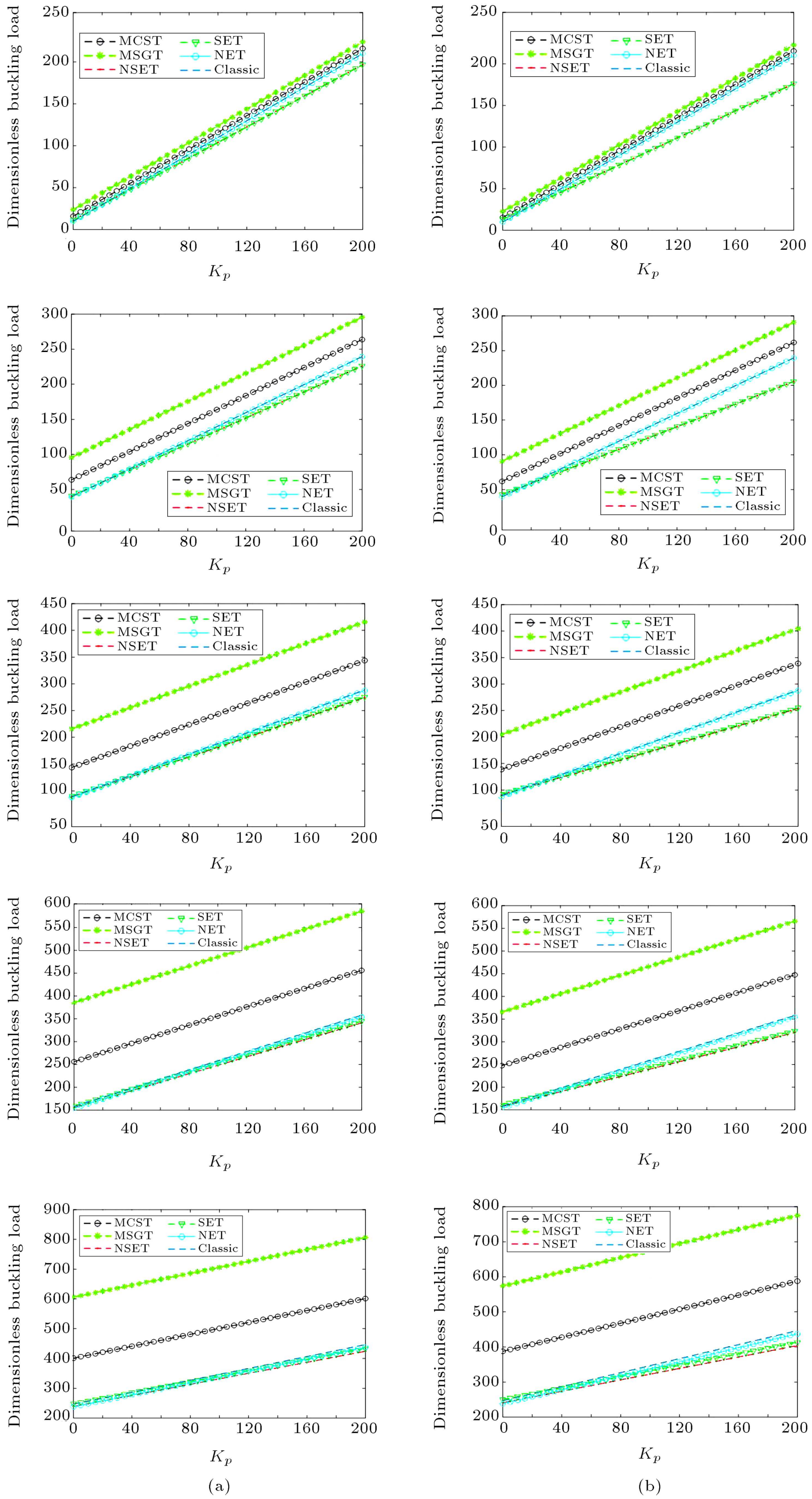

Figure 10. Buckling analysis results with a change in Pasternak foundation for the first five modes (a) BNNT and (b) SiCNT.

Table 1. Dimensionless critical buckling load of nanostructures with various foundation and theory parameters.

		Elastic foundation parameters (K_w, K_p)							
		(0, 0)	(0, 0.5 π^2)	(0, 2.5 π^2)	(1, 0)	(10^2, π^2)	(10^4, π^2)	(10^4, 2.5 π^2)	(10^6, 2.5 π^2)
MCST	l2 = 0.1 nm	9.87105	14.80585	34.5451	9.97237	29.8728	211.288	226.093	2024.990
	l2 = 0.5 nm	9.90562	14.84043	34.5796	10.0069	29.9073	211.599	226.404	2028.448
	l2 = 1 nm	10.0137	14.94849	34.6877	10.1150	30.0154	212.572	227.376	2039.254
SET	E^s = 20 N/m	10.0032	14.9380	34.6772	10.1045	30.0049	212.444	227.249	2037.794
	E^s = 35.3 N/m	10.1022	15.0370	34.7762	10.2035	30.1039	213.335	228.140	2047.696
	E^s = 50 N/m	10.1973	15.1321	34.8714	10.2986	30.1991	214.191	228.996	2057.210
MSGT	l = 0.1 nm	9.87532	14.81012	34.5493	9.97664	29.8770	211.371	226.176	2031.577
	l = 0.5 nm	10.0124	14.94723	34.6864	10.1138	30.0142	213.680	228.485	2193.108
	l = 1 nm	10.4409	15.37571	35.1149	10.5422	30.4426	220.896	235.701	2678.936
NET	e_0a = 0.5 nm	9.85441	14.78921	34.5284	9.9557	29.8561	210.059	224.864	1892.980
	e_0a = 1 nm	9.80910	14.74390	34.4831	9.9104	29.8108	206.603	221.408	1648.308
	e_0a = 10 nm	6.10422	11.03902	30.7782	6.2055	26.1059	136.007	150.811	1053.631
FEM N=4	e_0a = 0.5 nm	9.8594	14.7942	34.5335	9.9608	29.8611	212.3340	227.1384	2289.322
	e_0a = 1 nm	9.8141	14.7489	34.4881	9.9154	29.8157	208.5095	223.3139	1600.00
	e_0a = 10 nm	6.1061	11.0410	30.7802	6.2075	26.1059	132.9205	147.7249	1089.396
FEM N=9	e_0a = 0.5 nm	9.8546	14.7894	34.5286	9.9559	29.8563	210.1890	224.9934	1972.864
	e_0a = 1 nm	9.8093	14.7441	34.4833	9.9106	29.8110	206.7157	221.5201	1639.829
	e_0a = 10 nm	6.1043	11.0391	30.7783	6.2056	26.1059	135.8585	150.6626	1072.55
FEM N=20	e_0a = 0.5 nm	9.8544	14.7892	34.5284	9.9557	29.8561	210.059	224.864	1892.980
	e_0a = 1 nm	9.8091	14.7439	34.4831	9.9104	29.8108	206.603	221.408	1648.308
	e_0a = 10 nm	6.1042	11.0390	30.7782	6.2055	26.1059	136.007	150.811	1053.631
Classic	Present results	9.8696	14.804	34.544	9.9709	29.871	211.275	226.079	2024.846
	Naidu and Rao [112]	9.8696	14.804	34.544	9.9709	29.871	211.28	226.09	2031.9
	FEM results ($N = 4$)	9.8747	14.8095	34.5487	9.9760	29.8763	213.6808	228.4852	2472.769
	Comsol results	9.86963	14.80434	34.54426	9.97094	29.87136	211.27554	226.08113	2024.88614

were calculated for the maximum fifth mode. To validate the calculations, comparative results with those in the literature are given in the table. Comparative results were in good harmony. To conclude, based on the small-scale theories used in the study, the highest buckling loads were obtained in the case of modified strain gradient theories used and the lowest in the case of nonlocal elasticity theory. Furthermore, the effect of foundation on buckling reduced with an increase in the number of modes.

Acknowledgements

This study has been supported by The Scientific and Technological Research Council of Turkey (TÜBİTAK) with Project No. 117M495. This support is gratefully acknowledged.

References

1. Lin, H.R., Zhou, C.K., Tian, Y., et al. "Bulk assembly of organic metal halide nanotubes", *Chem Sci*, **8**(12), pp. 8400-8404 (2017).
2. Moaseri, E., Karimi, M., Bazubandi, B., et al. "Alignment of carbon nanotubes in bulk epoxy matrix using a magnetic-assisted method: Solenoid magnetic field", *Polym Sci Ser a+*, **59**(5), pp. 726-733 (2017).
3. Zhao, X.L., Zhang, S.C., Zhu, Z.X., et al. "Catalysts for single-wall carbon nanotube synthesis From surface growth to bulk preparation", MRS Bull, **42**(11), pp. 809-818 (2017).
4. Mishra, R.K., Mishra, P., Verma, K., et al. "Manipulation of thermo-mechanical, morphological and electrical properties of PP/PET polymer blend using MWCNT as nano compatibilizer: A comprehensive study of hybrid nanocomposites", *Vacuum*, **157**, pp. 433-441 (2018).
5. Li, Q., Rottmair, C.A., and Singer, R.F. "CNT reinforced light metal composites produced by melt stirring and by high pressure die casting", *Compos Sci Technol*, **70**(16), pp. 2242-2247 (2010).
6. Calbi, M.M., Toigo, F., and Cole, M.W. "Dilation-induced phases of gases absorbed within a bundle of carbon nanotubes", *Phys Rev Lett*, **86**(22), pp. 5062-5065 (2001).
7. Lalwani, G., Kwaczala, A.T., Kanakia, S., et al. "Fab-

rication and characterization of three-dimensional macroscopic all-carbon scaffolds", *Carbon*, **53**, pp. 90-100 (2013).

8. Valenti, G., Boni, A., Melchionna, M., et al. "Co-axial heterostructures integrating palladium/titanium dioxide with carbon nanotubes for efficient electrocatalytic hydrogen evolution", *Nat Commun*, **7**, pp. 1-8 (2016).
9. Iijima, S. "Helical microtubules of graphitic carbon", *Nature*, **354**(6348), pp. 56-58 (1991).
10. Watson, J.H. and Kaufmann, K. "Electron microscope examination of the microphysical properties of the polymer cuprene", *Journal of Applied Physics*, **17**(12), pp. 996-1005 (1946).
11. Radushkevich, L. and Lukyanovich, V. "About the structure of carbon formed by thermal decomposition of carbon monoxide on iron substrate", *J. Phys. Chem.(Moscow)*, **26**, pp. 88-95 (1952).
12. Bacon, R. "Growth, structure, and properties of graphite whiskers", *Journal of Applied Physics*, **31**(2), pp. 283-290 (1960).
13. Oberlin, A., Endo, M., and Koyama, T. "Filamentous growth of carbon through benzene decomposition", *J Cryst Growth*, **32**(3), pp. 335-349 (1976).
14. Abrahamson, J., Wiles, P.G., and Rhoades, B.L. "Structure of carbon fibers found on carbon arc anodes", *Carbon*, **37**(11), pp. 1873-1874 (1999).
15. Kolesnik, N.F., Akhmatov, Y.S., and Shomlin, V.I. "Metals", Izvestiya Akademii Nauk SSSR, **3**, pp. 12-17 (1982).
16. Reibold, M., Paufler, P., Levin, A.A., et al. "Materials - carbon nanotubes in an ancient damascus sabre", *Nature*, **444**(7117), p. 286 (2006).
17. Ding, C.Y., Wang, L.J., Zhou, W.W., et al. "New design on Li-ion battery anode of ternary complex metal/metal oxide@CNT: A case study of hierarchical NiCo-NiCo2O4@CNTs", *Chem Eng J*, **353**, pp. 340-349 (2018).
18. Kazazi, M., Zafar, Z.A., Delshad, M., et al. "TiO2/CNT nanocomposite as an improved anode material for aqueous rechargeable aluminum batteries", *Solid State Ionics*, **320**, pp. 64-69 (2018).
19. Kesavan, T., Gunawardhana, N., Senthil, C., et al. "Fabrication of hollow Co3O4 nanospheres and their nanocomposites of CNT and rGO as high-performance anodes for lithium-ion batteries", *Chemistryselect*, **3**(20), pp. 5502-5511 (2018).
20. Lakshmi-Narayana, A., Dhananjaya, M., Guru-Prakash, N., et al. "Li2TiO3/Graphene and Li2TiO3/CNT composites as anodes for high power Li-Ion batteries", *Chemistryselect*, **3**(31), pp. 9150-9158 (2018).
21. Park, B.H., Roh, H.K., Haghighat-Shishavan, S., et al. "Silicon diphosphide-CNT composite anode material for high-performance Li-ion batteries", *Abstr Pap Am Chem S*, **256** (2018).
22. Peng, T., Guo, W., Zhang, Q., et al. "Uniform coaxial CNT@Li2MnSiO4@C as advanced cathode material for lithium-ion battery", *Electrochim Acta*, **291**, pp. 1-8 (2018).
23. Razaq, R., Sun, D., Xin, Y., et al. "Enhanced kinetics of polysulfide redox reactions on Mo2C/CNT in lithium-sulfur batteries", *Nanotechnology*, **29**(29) (2018).
24. Wang, D., Guo, J., Cui, C.Y., et al. "Controllable synthesis of CNT@ZnO composites with enhanced electrochemical properties for lithium-ion battery", *Mater Res Bull*, **101**, pp. 305-310 (2018).
25. Wang, D.X., Li, D., Muhammad, J., Zhou, Y.L., et al. "Buildup of Sn@CNT nanorods by in-situ thermal plasma and the electronic transport behaviors", *Sci China Mater*, **61**(12), pp. 1605-1613 (2018).
26. Wang, J.F., Li, H.R., Xu, N.N., et al. "Optimization of rechargeable zinc-air battery with Co3O4/MnO2/CNT bifunctional catalyst: effects of catalyst loading, binder content, and spraying area", *Ionics*, **24**(12), pp. 3877-3884 (2018).
27. Yuan, J.J., Zheng, X.K., Jiang, L., et al. "CNT-intercalated rGO/sulfur laminated structure for high-rate and long-life lithium-sulfur batteries", *Mater Lett*, **219**, pp. 68-71 (2018).
28. Zhang, X., Wang, C.Y., Li, H.H., et al. "High performance Li-CO2 batteries with NiO-CNT cathodes", *J Mater Chem A*, **6**(6), pp. 2792-2796 (2018).
29. Peng, S., Cho, K.J., Qi, P.F., et al. "Ab initio study of CNT NO2 gas sensor", *Chem Phys Lett*, **387**(4-6), pp. 271-276 (2004).
30. Kim, S. "CNT sensors for detecting gases with low adsorption energy by ionization", *Sensors-Basel*, **6**(5), pp. 503-513 (2006).
31. Kim, S.J. "The effect on the gas selectivity of CNT-based gas sensors by binder in SWNT/Silane sol solution", *IEEE Sens J*, **10**(1), pp. 173-177 (2010).
32. Srivastava, S., Sharma, S.S., Agrawal, S., et al. "Study of chemiresistor type CNT doped polyaniline gas sensor", *Synthetic Met*, **160**(5-6), pp. 529-534 (2010).
33. Leghrib, R., Felten, A., Pireaux, J.J., et al. "Gas sensors based on doped-CNT/SnO2 composites for NO2 detection at room temperature", *Thin Solid Films*, **520**(3), pp. 966-970 (2011).
34. Lee, H., Lee, S., Kim, D.H., et al. "Integrating metal-oxide-decorated CNT networks with a CMOS readout in a gas sensor", *Sensors-Basel*, **12**(3), pp. 2582-2597 (2012).
35. Istadeh, K.H., Kalantarinejad, R., Aghaei, M.J., et al. "Computational Investigation on H2S Adsorption on the CNT Channel of Conductometric Gas Sensor", *J Comput Theor Nanos*, **10**(11), pp. 2708-2713 (2013).
36. Park, S.J., Kwon, O.S., and Jang, J. "A high-performance hydrogen gas sensor using ultrathin polypyrrole-coated CNT nanohybrids", *Chem Commun*, **49**(41), pp. 4673-4675 (2013).

37. Majumdar, S., Nag, P., and Devi, P.S. "Enhanced performance of CNT/SnO2 thick film gas sensors towards hydrogen", *Mater Chem Phys*, **147**(1-2), pp. 79-85 (2014).

38. Mittal, M. and Kumar, A. "Carbon nanotube (CNT) gas sensors for emissions from fossil fuel burning", *Sensor Actuat B-Chem*, **203**, pp. 349-362 (2014).

39. Kamble, V. and Umarji, A. "Analyzing the kinetic response of tin oxide-carbon and tin oxide-CNT composites gas sensors for alcohols detection", *Aip Adv*, **5**(3), pp. 1-9 (2015).

40. Rahman, R. and Servati, P. "Efficient analytical model of conductivity of CNT/polymer composites for wireless gas sensors", *IEEE T Nanotechnol*, **14**(1), pp. 118-129 (2015).

41. Donaldson, L. "CNT sensors that can detect toxic gases", *Mater Today*, **19**(9), pp. 489-490 (2016).

42. Alshammari, A.S., Alenezi, M.R., Lai, K.T., et al. "Inkjet printing of polymer functionalized CNT gas sensor with enhanced sensing properties", *Mater Lett*, **189**, pp. 299-302 (2017).

43. Guo, T., Zhou, T.H., Tan, Q.L., et al. "A room-temperature CNT/Fe3O4 based passive wireless gas sensor", *Sensors-Basel*, **18**(10), pp. 1-11 (2018).

44. Shen, S.M., Fan, Z.H., Deng, J.H., et al. "An LC Passive Wireless Gas Sensor Based on PANI/CNT Composite", *Sensors-Basel*, **18**(9), pp. 1-13 (2018).

45. Zanjani, S.M.A., Dousti, M., and Dolatshahi, M. "High-precision, resistor less gas pressure sensor and instrumentation amplifier in CNT technology", *Aeu-Int J Electron C*, **93**, pp. 325-336 (2018).

46. Mercan, K. "A Comparative buckling analysis of silicon carbide nanotube and boron nitride nanotube", *International Journal of Engineering & Applied Sciences*, **8**(4), pp. 99-107 (2016).

47. Mercan, K. and Civalek, Ö. "DSC method for buckling analysis of boron nitride nanotube (BNNT) surrounded by an elastic matrix", *Composite Structures*, **143**, pp. 300-309 (2016).

48. Mercan, K. and Civalek, Ö. "Buckling analysis of silicon carbide nanotubes (SiCNTs)", *International Journal of Engineering & Applied Sciences*, **8**(2), pp. 101-108 (2016).

49. Li, T., Tang, Z.N., Huang, Z.X., et al. "A comparison between the mechanical and thermal properties of single-walled carbon nanotubes and boron nitride nanotubes", *Physica E*, **85**, pp. 137-142 (2017).

50. Petrushenko, I.K. and Petrushenko, K.B. "Mechanical properties of carbon, silicon carbide, and boron nitride nanotubes: effect of ionization", *Monatsh Chem*, **146**(10), pp. 1603-1608 (2015).

51. Darwish, A.A., Hassan, M.H., Abou Mandour, M.A., et al. "Mechanical properties of defective double-walled boron nitride nanotubes for radiation shielding applications: A computational study", *Comp Mater Sci*, **156**, pp. 142-147 (2019).

52. Mercan, K. and Civalek, Ö. "Buckling analysis of Silicon carbide nanotubes (SiCNTs) with surface effect and nonlocal elasticity using the method of HDQ", *Composites Part B: Engineering*, **114**, pp. 34-45 (2017).

53. Mercan, K., Numanoglu, H., Akgöz, B., et al. "Higher-order continuum theories for buckling response of silicon carbide nanowires (SiCNWs) on elastic matrix", *Archive of Applied Mechanics*, **87**(11), pp. 1797-1814 (2017).

54. Xu, H., Wang, Q., Fan, G.H., et al. "Theoretical study of boron nitride nanotubes as drug delivery vehicles of some anticancer drugs", *Theor Chem Acc*, **137**(7), pp. 1-15 (2018).

55. Niskanen, J., Zhang, I., Xue, Y.M., et al. "Boron nitride nanotubes as vehicles for intracellular delivery of fluorescent drugs and probes", *Nanomedicine-Uk*, **11**(5), pp. 447-463 (2016).

56. Ferreira, T.H., Faria, J.A.Q.A., Gonzalez, I.J., et al. "BNNT/Fe3O4 system as an efficient tool for magnetohyperthermia therapy", *J Nanosci Nanotechno*, **18**(10), pp. 6746-6755 (2018).

57. Srivastava, P., Sharma, V., and Jaiswal, N.K. "Adsorption of COCl2 gas molecule on armchair boron nitride nanoribbons for nano sensor applications", *Microelectron Eng*, **146**, pp. 62-67 (2015).

58. Song, J.X., Liu, H.X., and Shen, W.J. "Dependence of electronic structures of multi-walled boron nitride nanotubes on layer numbers", *Eur Phys J D*, **72**(10), pp. 1-8 (2018).

59. Schulz, M., Shanov, V., and Yin, Z., *Nanotube Superfiber Materials: Changing Engineering Design*, William Andrew (2013).

60. Zhou, M., Lu, Y.-H., Cai, Y.-Q., et al. "Adsorption of gas molecules on transition metal embedded graphene: a search for high-performance graphene-based catalysts and gas sensors", *Nanotechnol*, **22**(38), p. 385502 (2011).

61. Feng, J.-W., Liu, Y.-J., Wang, H.-X., et al. "Gas adsorption on silicene: a theoretical study", *Comp Mater Sci*, **87**, pp. 218-226 (2014).

62. Wu, R., Yang, M., Lu, Y., et al. "Silicon carbide nanotubes as potential gas sensors for CO and HCN detection", *J Phys Chem C*, **112**(41), pp. 15985-15988 (2008).

63. Huang, J. and Wan, Q. "Gas sensors based on semiconducting metal oxide one-dimensional nanostructures", *Sensors*, **9**(12), pp. 9903-9924 (2009).

64. Akgoz, B. and Civalek, O. "A new trigonometric beam model for buckling of strain gradient microbeams", *Int J Mech Sci*, **81**, pp. 88-94 (2014).

65. Gurses, M., Akgoz, B., and Civalek, O. "Mathematical modeling of vibration problem of nano-sized annular sector plates using the nonlocal continuum theory via eight-node discrete singular convolution transformation", *Appl Math Comput*, **219**(6), pp. 3226-3240 (2012).

66. Civalek, O. and Akgoz, B. "Free vibration analysis of microtubules as cytoskeleton components: non local Euler-Bernoulli beam modeling", *Sci Iran Trans B*, **17**(5), pp. 367-375 (2010).

67. Mercan, K. "A comparative buckling analysis of silicon carbide nanotube and boron nitride nanotube", *Int J Eng Appl Sci*, **8**(4), pp. 99-107 (2016).

68. Mercan, K. and Civalek, O. "Buckling analysis of Silicon carbide nanotubes (SiCNTs) with surface effect and nonlocal elasticity using the method of HDQ", *Compos Part B-Eng*, **114**, pp. 35-45 (2017).

69. Mercan, K. and Civalek, O. "DSC method for buckling analysis of boron nitride nanotube (BNNT) surrounded by an elastic matrix", *Compos Struct*, **143**, pp. 300-309 (2016).

70. Kiani, K. "Nonlocal Timoshenko beam for vibrations of magnetically affected inclined single-walled carbon nanotubes as nanofluidic conveyors", *Acta Phys Pol A*, **131**(6), pp. 1439-1444 (2017).

71. Jiang, J.N. and Wang, L.F. "Timoshenko beam model for vibrational analysis of double-walled carbon nanotubes bridged on substrate", *Curr Appl Phys*, **17**(12), pp. 1670-1690 (2017).

72. Demir, C., Mercan, K., Numanoglu, H.M., et al. "Bending response of nanobeams resting on elastic foundation", *Journal of Applied and Computational Mechanics*, **4**(2), pp. 105-114 (2018).

73. Avcar, M. and Mohammed, W.K.M. "Free vibration of functionally graded beams resting on Winkler-Pasternak foundation", *Arab J Geosci*, **11**(10), pp. 1-8 (2018).

74. Civalek, O. "The determination of frequencies of laminated conical shells via the discrete singular convolution method", *J Mech Mater Struct*, **1**(1), pp. 163-182 (2006).

75. Civalek, O. and Akgoz, B. "Vibration analysis of micro-scaled sector shaped graphene surrounded by an elastic matrix", *Comp Mater Sci*, **77**, pp. 295-303 (2013).

76. Baltacioglu, A.K., Civalek, O., Akgoz, B., et al. "Large deflection analysis of laminated composite plates resting on nonlinear elastic foundations by the method of discrete singular convolution", *Int J Pres Ves Pip*, **88**(8-9), pp. 290-300 (2011).

77. Baltacioglu, A.K., Akgoz, B., and Civalek, O. "Nonlinear static response of laminated composite plates by discrete singular convolution method", *Compos Struct*, **93**(1), pp. 153-161 (2010).

78. Avcar, M. "Effects of material non-homogeneity and two parameter elastic foundation on fundamental frequency parameters of Timoshenko beams", *Acta Phys Pol A*, **130**(1), pp. 375-378 (2016).

79. Avcar, M. "Effects of rotary inertia shear deformation and non-homogeneity on frequencies of beam", *Struct Eng Mech*, **55**(4), pp. 871-884 (2015).

80. Fleck, N. and Hutchinson, J. "Strain gradient plasticity", *Adv Appl Mech*, **33**, pp. 296-361 (1997).

81. Yang, F., Chong, A., Lam, D.C., et al. "Couple stress based strain gradient theory for elasticity", *Int J Solids Struct*, **39**(10), pp. 2731-2743 (2002).

82. Ma, H., Gao, X.-L., and Reddy, J. "A microstructure-dependent Timoshenko beam model based on a modified couple stress theory", *J Mech Phys Solids*, **56**(12), pp. 3379-3391 (2008).

83. Reddy, J. "Microstructure-dependent couple stress theories of functionally graded beams", *J Mech Phys Solids*, **59**(11), pp. 2382-2399 (2011).

84. Zhou, S. and Li, Z. "Length scales in the static and dynamic torsion of a circular cylindrical micro-bar", *J Shandong Univ Technol*, **31**(5), pp. 401-407 (2001).

85. Akgöz, B. and Civalek, Ö. "Buckling analysis of cantilever carbon nanotubes using the strain gradient elasticity and modified couple stress theories", *J Comput Theor Nanos*, **8**(9), pp. 1821-1827 (2011).

86. Akgöz, B. and Civalek, Ö. "Longitudinal vibration analysis for microbars based on strain gradient elasticity theory", *J Vib Control*, **20**(4), pp. 606-616 (2014).

87. Akgöz, B. and Civalek, Ö. "Shear deformation beam models for functionally graded microbeams with new shear correction factors", *Compos Struct*, **112**, pp. 214-225 (2014).

88. Asghari, M., Kahrobaiyan, M., and Ahmadian, M. "A nonlinear Timoshenko beam formulation based on the modified couple stress theory", *Int J Eng Sci*, **48**(12), pp. 1749-1761 (2010).

89. Eringen, A.C. "On differential equations of nonlocal elasticity and solutions of screw dislocation and surface waves", *J Appl Phys*, **54**(9), pp. 4703-4710 (1983).

90. Eringen, A.C., *Nonlocal Continuum Field Theories*, Springer Science & Business Media (2002).

91. Dingreville, R., Qu, J., and Cherkaoui, M. "Surface free energy and its effect on the elastic behavior of nano-sized particles, wires and films", *J Mech Phys Solids*, **53**(8), pp. 1827-1854 (2005).

92. Mercan, K. and Civalek, Ö. "Buckling Analysis of Silicon Carbide Nanotubes (SiCNTs)", *International Journal of Engineering & Applied Sciences (IJEAS)*, **8**(2), pp. 101-108 (2016).

93. Rahmani, O., Asemani, S., and Hosseini, S. "Study the surface effect on the buckling of nanowires embedded in Winkler-Pasternak elastic medium based on a nonlocal theory", *J Nanostructures*, **6**(1), pp. 90-95 (2016).

94. Sharma, P. and Ganti, S. "Size-dependent Eshelby's tensor for embedded nano-inclusions incorporating surface/interface energies", *J Appl Mech*, **71**(5), pp. 663-671 (2004).

95. Sharma, P., Ganti, S., and Bhate, N. "Effect of surfaces on the size-dependent elastic state of nano-inhomogeneities", *Appl Phys Lett*, **82**(4), pp. 535-537 (2003).

96. Ansari, R., Rouhi, S., Aryayi, M., et al. "On the buckling behavior of single-walled silicon carbide nanotubes", *Sci Iran*, **19**(6), pp. 1984-1990 (2012).

97. Arani, A.G. and Hashemian, M. "Surface stress effects on dynamic stability of double-walled boron nitride nanotubes conveying viscose fluid based on nonlocal shell theory", *Sci Iran*, **20**(6), pp. 2356-2374 (2013).

98. Saljooghi, R., Ahmadiana, M.T., and Farrahi, G.H. "Vibration and buckling analysis of functionally graded beams using reproducing kernel particle method", *Sci Iran*, **21**(6), pp. 1896-1906 (2014).

99. Darvizeh, M., Darvizeh, A., Ansari, R., et al. "Pre- and post-buckling analysis of functionally graded beams subjected to statically mechanical and thermal loads", *Sci Iran*, **22**(3), pp. 778-791 (2015).

100. Shooshtari, A. and Dalir, M.A. "Nonlinear free vibration analysis of clamped circular fiber metal laminated plates", *Sci Iran*, **22**(3), pp. 813-824 (2015).

101. Ansari, R. and Gholami, R. "Nonlocal nonlinear first-order shear deformable beam model for post-buckling analysis of magneto-electro-thermo-elastic nanobeams", *Sci Iran*, **23**(6), pp. 3099-3114 (2016).

102. Rouzegar, J. and Sharifpoor, R.A. "Finite element formulations for free vibration analysis of isotropic and orthotropic plates using two-variable refined plate theory", *Sci Iran*, **23**(4), pp. 1787-1799 (2016).

103. Refaeinejad, V., Rahmani, O., and Hosseini, S.A.H. "An analytical solution for bending, buckling, and free vibration of FG nanobeam lying on Winkler-Pasternak elastic foundation using different nonlocal higher order shear deformation beam theories", *Sci Iran*, **24**(3), pp. 1635-1653 (2017).

104. Jabbarian, S. and Ahmadian, M.T. "Free vibration analysis of functionally graded stiffened micro-cylinder based on the modified couple stress theory", *Sci Iran*, **25**(5), pp. 2598-2615 (2018).

105. Sahoo, S.S., Hirwani, C.K., Panda, S.K., et al. "Numerical analysis of vibration and transient behaviour of laminated composite curved shallow shell structure: An experimental validation", *Sci Iran*, **25**(4), pp. 2218-2232 (2018).

106. COMSOL Multiphysics® v. 5.2. www.comsol.com. COMSOL AB, Stockholm, Sweden.

107. ANSYS® Academic Research Mechanical.

108. Jalan, S.K., Rao, B.N., and Gopalakrishnan, S. "Vibrational characteristics of zigzag, armchair and chiral cantilever single-walled carbon nanotubes", *Adv Compos Lett*, **22**(6), pp. 131-142 (2013).

109. Gurtin, M.E. and Murdoch, A.I. "A continuum theory of elastic material surfaces", *Archive for Rational Mechanics and Analysis,* **57**(4), pp. 291-323 (1975).

110. Gurtin, M.E. and Murdoch, A.I. "Surface Stress in Solids", *Int J Solids Struct*, **14**(6), pp. 431-440 (1978).

111. Civalek, O. and Demir, C. "A simple mathematical model of microtubules surrounded by an elastic matrix by nonlocal finite element method", *Appl Math Comput*, **289**, pp. 335-352 (2016).

112. Naidu, N. and Rao, G. "Vibrations of initially stressed uniform beams on a two-parameter elastic foundation", *Comp Struct*, **57**(5), pp. 941-943 (1995).

Biographies

Hayri Metin Numanoğlu currently works on his MSc thesis on nanocaled mechanics in Akdeniz University Civil Engineering Department. His research interest lies in vibration analysis of nano- and micro-scaled continuous components by analytical and finite element methods.

Kadir Mercan graduated from Süleyman Demirel University Civil Engineering program in 2013 with first degree. He is currently working as a Research Assistant at Mehmet Akif Ersoy University, Architecture and Engineering Faculty, Civil Engineering Department, Mechanical Division. He is currently studying PhD degree under the advice of Prof. Ömer Civalek at Akdeniz University following obtaining a master degree.

Ömer Civalek is an Professor at the Faculty of Engineering, University of Akdeniz. He holds two PhD Degrees in Structural and Mechanical Engineering, one from Dokuz Eylül University in Structural Engineering and the other from the University of Fırat in Applied Mechanics. He has authored 220 refereed journal papers (about 125 in SCI Journals) with 6000 citations, over 30 papers presented at various conferences, and 40 papers in various national journals. His research emphasis has been on solid mechanics, vibration, buckling analyses of plates and shells, computational mechanics, modeling of nanostructures, and composites mechanics.